

# Complex-variable MP2 theory applied to core-vacant states for the computation of Auger spectra

Florian Matz,<sup>1</sup> Jan Philipp Drennhaus,<sup>1</sup> Anthuan Ferino-Pérez,<sup>1</sup> and Thomas-C. Jagau<sup>1</sup>  
*Department of Chemistry, KU Leuven, B-3001 Leuven, Belgium*

(\*Electronic mail: thomas.jagau@kuleuven.be)

(Dated: 13 June 2025)

We model Auger spectra using second-order Møller-Plesset perturbation (MP2) theory combined with complex-scaled basis functions. For this purpose, we decompose the complex MP2 energy of the core-hole state into contributions from specific decay channels and propose a corresponding equation-of-motion (EOM) method for computing the doubly ionized final states of Auger decay. These methods lead to significant savings in computational cost compared to our recently developed approaches based on coupled-cluster theory [J. Chem. Phys. 156, 114117 (2022)].

The test set for this study comprises water, ammonia, methane, hydrogen sulfide, phosphine, and silane. The energies of the final states of Auger decay are obtained with an accuracy comparable to EOM coupled-cluster singles and doubles (CCSD) theory. Partial decay widths and branching ratios between KLL, KLM, and KMM decay of K-shell holes in third-row hydrides are in good agreement with EOM-CCSD, while deviations are more significant for second-row hydrides. For L<sub>1</sub>-shell holes, which undergo Coster-Kronig decay, MP2 yields unphysical results. However, we show that a suitable shift of the MP2 energy denominators leads to more reliable branching ratios and spectra for these problematic cases.

## I. Introduction

Auger decay<sup>1</sup> is a relaxation process of core-vacant states in which a weaker bound electron refills the core vacancy while a second electron, the Auger electron, is emitted. It is the dominating decay process for core vacancies in molecules composed of light nuclei. Core-vacant states are produced under X-ray irradiation,<sup>1–3</sup> by collisions with high-energy electrons,<sup>4</sup> or by electron capture by unstable nuclei.<sup>5</sup> The measurement of the energy distribution of Auger electrons allows to record Auger spectra that provide a variety of chemical information about molecules,<sup>6–15</sup> clusters,<sup>16</sup> and nanostructures.<sup>17,18</sup> Auger electrons are also relevant for radiomedicine.<sup>19,20</sup>

While Auger decay can occur in atoms as light as lithium, beryllium, and boron<sup>21</sup>, spectroscopic and radiotherapeutic interest lies in heavier nuclei with many possible final electronic states in a large range of energies.<sup>8,14,19,20,22</sup> Furthermore, Auger decay not only takes place in small isolated molecules, but is often studied in large molecules, species embedded in solvents or matrices, or in solids.<sup>17,18,23,24</sup>

It is common practice to use the X-ray notation to name Auger spectra according to the shells of the involved electrons. A KLL spectrum, for example, includes channels where a vacancy in the K-shell (1s) gets filled by an electron from the L-shell (2s and 2p), while a second electron from the same shell is emitted. The L-shell and the M-shell are split into subshells: the lowest orbital in each shell is labeled by the index 1 (L<sub>1</sub>, M<sub>1</sub>) and the higher-lying 3 orbitals by the index 2,3 (L<sub>2,3</sub>, M<sub>2,3</sub>).

Computational modeling of Auger decay is often a necessary supplement to experiments because it allows definitive assignment of signals to channels and electronic configurations.<sup>13,14,25</sup> An important feature of Auger decay is that it requires special quantum-mechanical methods to handle the coupling to the continuum.<sup>26–28</sup>

One can distinguish between methods that only aim at the

energy of the Auger electrons and methods where the decay channels' intensities are explicitly calculated, allowing the prediction of peak heights and shapes in the spectrum. To account for the decay and compute partial widths for the decay channels, different methods have been proposed. One approach is Fano's theory,<sup>29–39</sup> which either requires an explicit treatment of the emitted electron or a treatment in terms of Stieltjes imaging.<sup>40</sup> Often, the core-valence separation (CVS) is applied to the core-vacant state.<sup>41–43</sup> A possible approach to facilitating calculations based on Fano's theory is the one-center approximation.<sup>44–47</sup>

Recently, a different method has been introduced for modeling Auger decay,<sup>27,48–52</sup> where the outgoing electron is described implicitly through complex scaling of the coordinates in the Hamiltonian<sup>26,53,54</sup> or the basis functions.<sup>55,56</sup> This scaling has the effect that the wave functions of decaying states become  $L^2$  integrable and can be treated by standard quantum-chemical methods.<sup>57–63</sup> The eigenenergies become complex and their imaginary part is related to the decay width of the respective state, which is inversely proportional to the lifetime. The partial widths can be computed via decomposition of the energy<sup>27</sup> or by restricting the excitation manifold by Auger Channel Projectors.<sup>48</sup>

The current approaches to Auger decay based on complex-variable methods use coupled-cluster theory with single and double substitutions (CCSD). The largest systems to which we applied these methods so far are benzene<sup>50</sup> and the zinc atom.<sup>52</sup> This limited scope is a consequence of the large basis sets that need to be employed in complex-variable calculations.<sup>27</sup> It is evident that a more economical method is necessary for the description of Auger decay in larger molecules. Recently, we investigated the performance of the configuration interaction singles (CIS) method for the description of Auger decay.<sup>48</sup> This method yields reliable results, but a drawback is the need to run calculations based on several different reference states, which is inconvenient and can lead to internal inconsistencies.

In this work, we explore the performance of complex-variable second-order Møller-Plesset perturbation (MP2) theory for the description of Auger decay in several hydrides of second-row and third-row elements. In third-row elements, core holes can be created in the K-shell and in the L-shell, and the decay can involve electrons from the L and M shells, giving rise to several energetically separate branches of the spectrum for each core hole.

The MP2 method is well established for the computation of core-ionization energies.<sup>64–70</sup> In a recent study, some of us combined MP2 with complex-scaled basis functions to describe Auger decay in the hexaaquazinc(II) complex.<sup>52</sup> In the present work, we provide a more comprehensive assessment of the method.

In addition to the computation of total and partial Auger decay widths with complex-variable MP2 theory, we also propose a second-order perturbative correction to the equation-of-motion (EOM) double ionization potential (DIP) CCSD method (EOMDIP-CCSD(2)) for computing the final states of Auger decay. Compared to EOMDIP-CCSD,<sup>71,72</sup> which is established for the computation of double ionization energies, this method circumvents the need to carry out a CCSD calculation on the reference state so that the overall calculation is less costly.

The remainder of this article is structured as follows: In Section II, a brief overview of the theoretical background and an explicit expression for the partial widths in MP2 theory are given. We also discuss why MP2 yields unphysical widths for several decay processes and how this problem can be fixed by a shift of the energy denominator. In Section III, the computational details are discussed, before results for K-edge ionization energies, decay widths, and Auger spectra of water, ammonia, and methane are presented in Section IV and of hydrogen sulfide, phosphine, and silane in Section V. Section VI discusses results for L<sub>1</sub>-edge ionization of third-row hydrides. The article ends with our general conclusions in Section VII.

## II. Theoretical considerations

The modeling of Auger spectra requires to compute partial decay widths for peak intensities and Auger electron energies for peak positions. The latter are obtained from the energy differences between the initial core-ionized and final doubly ionized states. We discuss the computation of widths and initial-state energies in Secs. II A and II B and that of final-state energies in Sec. II C.

### A. Computation of Auger decay widths with complex scaling

We compute decay widths by including complex-scaled functions of the form

$$\chi(r) = P(r) \exp[-\alpha e^{-2i\theta} (r - r_A)^2] \quad (1)$$

in a Gaussian basis set.<sup>55,60</sup> In Eq. (1),  $P(r)$  is a polynomial in the spatial coordinates,  $A$  is a nucleus, and  $\theta$  is the complex scaling angle. The choice of exponents  $\alpha$  for the complex-scaled functions has been extensively discussed in our previous works.<sup>27,48,51,52</sup> Details of the basis set employed in the present work are given in Section III.

In such a basis set, the molecular electronic Hamiltonian has eigenstates with complex energy

$$E_{\text{res}} = E_R - i\Gamma/2 \quad (2)$$

that correspond to resonances with energy  $E_R$  that decay with the width  $\Gamma$  corresponding to the lifetime  $1/\Gamma$ .<sup>26,73</sup> The method of complex basis functions (CBFs) is applicable not only to Auger decay, but also to temporary anions,<sup>60–62,74</sup> superexcited Rydberg states,<sup>75</sup> interatomic Coulombic decay,<sup>76</sup> and ionization in static electric fields.<sup>77,78</sup>

Our previous work on Auger decay<sup>27,48</sup> was based on coupled-cluster theory.<sup>79,80</sup> The wave function is expressed as

$$|\Psi_{\text{CC}}\rangle = e^{\hat{T}} |\Psi_0\rangle = (1 + \hat{T} + \hat{T}^2/2! + \hat{T}^3/3! + \dots) |\Psi_0\rangle. \quad (3)$$

Within the CCSD approximation, the excitation operator only includes single and double excitations,

$$\hat{T} = \hat{T}_1 + \hat{T}_2 = \sum_i^{n_{\text{occ}}} \sum_a^{n_{\text{virt}}} t_i^a a^\dagger i + \frac{1}{4} \sum_{ij}^{n_{\text{occ}}} \sum_{ab}^{n_{\text{virt}}} t_{ij}^{ab} a^\dagger i b^\dagger j \quad (4)$$

with  $i, j, \dots$  and  $a, b, \dots$  referring to occupied and virtual spin orbitals, respectively. For a CCSD wave function built on top of a core-ionized Hartree-Fock (HF) wave function  $|\Psi_0\rangle$  in a basis set with complex-scaled functions, we showed that Auger decay is represented by double excitations where  $i, j$  refer to valence orbitals and  $a$  or  $b$  is the core-ionized orbital. The CC energy

$$E_{\text{CC}} = E_{\text{HF}} + \sum_{ij}^{n_{\text{occ}}} \sum_{ab}^{n_{\text{virt}}} \left( \frac{1}{4} t_{ij}^{ab} + \frac{1}{2} t_i^a t_j^b \right) \langle ij || ab \rangle \quad (5)$$

computed from such a wave function is complex.

A complication arises from the dependence of the complex energy on the scaling angle  $\theta$ . While the energy is independent of  $\theta$  in a complete basis set,<sup>28</sup> it needs to be optimized for every state in a finite basis set. As suggested in previous works,<sup>56,81</sup> we do this by minimizing  $|\text{d}(E_{\text{CC}}^{\text{IP}} - E_{\text{CC}}^0)/\text{d}\theta|$  where  $E_{\text{CC}}^{\text{IP}}$  and  $E_{\text{CC}}^0$  are the CC energies of the core-ionized state and the neutral ground state. The values obtained for  $\theta$  in the present work are available from the Supporting Information. The total Auger decay width  $\Gamma$  is then evaluated at the optimal  $\theta$  according to Eq. (2) as

$$\Gamma = -2 \text{Im}(E_{\text{CC}}^{\text{IP}} - E_{\text{CC}}^0) \quad (6)$$

As shown in our previous work,<sup>27</sup> taking into account the imaginary part of the energy of the neutral ground state, which vanishes in the complete basis set limit, leads to markedly better results.

The partial width  $\gamma_{ij}(\mathbf{c})$  for decay into a particular channel defined by orbitals  $i$  and  $j$  can be computed as<sup>27</sup>

$$\gamma_{ij}^{\text{CCSD}}(\mathbf{c}) = -2 \text{Im} \left( \sum_a^{n_{\text{virt}}} (2t_i^a t_j^{\mathbf{c}} + t_{ij}^{a\mathbf{c}}) \langle ij || a\mathbf{c} \rangle \right) \quad (7)$$

where we have denoted the core orbital that is vacant in the initial state by a bold  $\mathbf{c}$ .

## B. Combination with MP2 theory

In this work, we extend our approach to second-order Møller-Plesset perturbation (MP2) theory. This is possible because the first-order wave function includes the doubly excited configurations that describe Auger decay when a core-ionized HF state is used as reference wave function. For a canonical HF reference, the MP2 energy reads

$$E_{\text{MP2}} = -\frac{1}{4} \sum_{ij}^{n_{\text{occ}}} \sum_{ab}^{n_{\text{virt}}} \frac{\langle ab||ij\rangle \langle ij||ab\rangle}{\epsilon_a + \epsilon_b - \epsilon_i - \epsilon_j} = -\frac{1}{4} \sum_{ij}^{n_{\text{occ}}} \sum_{ab}^{n_{\text{virt}}} t_{ij}^{ab} \langle ij||ab\rangle \quad (8)$$

with  $\epsilon_i$ ,  $\epsilon_j$  and  $\epsilon_a$ ,  $\epsilon_b$  as energies of occupied and virtual HF orbitals, respectively.

Eq. (8) is identical to Eq. (5) except for the absence of single excitations. From this, it follows that the total decay width can be computed from the imaginary part of the MP2 energy using Eq. (6), while partial widths can be evaluated as

$$\gamma_{ij}^{\text{MP2}}(\mathbf{c}) = -2 \text{Im} \left( \sum_a^{n_{\text{virt}}} \frac{\langle a\mathbf{c}||ij\rangle \langle ij||a\mathbf{c}\rangle}{\epsilon_a + \epsilon_{\mathbf{c}} - \epsilon_i - \epsilon_j} \right). \quad (9)$$

In our CC-based work on Auger decay, we distinguished the approach for partial widths based on Eq. (7) from an alternative method, dubbed Auger Channel Projector (ACP),<sup>48</sup> in which all excitations  $a^\dagger \mathbf{c}^\dagger ij$  contributing to a particular partial width  $\gamma_{ij}$  are excluded from the excitation manifold while the CC equations are solved. These two approaches become identical for the MP2 method since the amplitudes are not determined iteratively and thus do not depend on each other. In fact, partial widths can be computed from Eq. (9) without carrying out a full MP2 calculation: for describing the decay channel associated with orbitals  $i$  and  $j$ , only the integrals  $\langle ij||a\mathbf{c}\rangle$  need to be computed. Overall, the computational cost of the determination of the decay widths is decreased from iterative  $\mathcal{O}(N^6)$  for CCSD to non-iterative  $\mathcal{O}(N^5)$  for MP2.

As we will illustrate numerically in Secs. IV and VI, straightforward application of Eq. (9) leads to bad results in some cases. This can be understood by analyzing the energy differences relevant to Auger decay. In a one-electron picture using Koopmans' theorem, the Auger electron energy is

$$E_{\text{Auger}} = \epsilon_1 + \epsilon_2 - \epsilon_{\text{core}} \quad (10)$$

for a decay channel where an initial vacancy in  $\phi_{\text{core}}$  is filled by an electron from valence orbital  $\phi_1$  and a second electron is ejected from  $\phi_2$ .

Tab. I shows these energies for some representative examples of K-edge decay and  $L_1$ -edge decay. In addition, the Auger electron energies from EOM-CCSD calculations are shown. Tab. I illustrates that Auger electron energies computed from a  $L_1$ -ionized HF wave function according to Eq. (10), with  $\epsilon_{\text{core}}$  as energy of the unoccupied core orbital, are negative. This is qualitatively wrong as it implies that the respective decay channels are closed. This failure can be ascribed in part to an underestimation of the core-ionization energy, but more importantly to the too high energies of the doubly-ionized states. These are caused by reduced screening of the nuclear charges in the core-ionized wave function, resulting in valence orbital energies that do not approximate the

TABLE I. Comparison of energies relevant for selected Auger decay channels of various molecules as computed at the HF and EOM-CCSD levels of theory using the cc-pCVTZ basis set augmented by additional complex-scaled shells.<sup>a</sup> All values in eV.

|   | H <sub>2</sub> S/L <sub>1</sub> | PH <sub>3</sub> /L <sub>1</sub> | SiH <sub>4</sub> /L <sub>1</sub> | H <sub>2</sub> O/K | H <sub>2</sub> S/K |
|---|---------------------------------|---------------------------------|----------------------------------|--------------------|--------------------|
| HF orbital energies, <sup>b</sup> ionized state |                                 |                                 |                                  |                    |                    |
| $\epsilon_{\text{core}}$                        | -224.9                          | -186.5                          | -151.5                           | -518.1             | -2440.8            |
| $\epsilon_1$                                    | -204.5                          | -168.4                          | -135.8                           | -51.7              | -282.2             |
| $\epsilon_2$                                    | -22.5                           | -21.2                           | -22.2                            | -33.8              | -231.7             |
| $\epsilon_1 + \epsilon_2$                       | -227.0                          | -189.6                          | -158.0                           | -85.5              | -513.9             |
| $E_{\text{Auger}}^c$                            | -2.1                            | -3.1                            | -6.5                             | 432.6              | 1926.9             |
| HF orbital energies, <sup>b</sup> neutral state |                                 |                                 |                                  |                    |                    |
| $\epsilon_{\text{core}}$                        | -244.0                          | -203.7                          | -166.5                           | -559.6             | -2502.5            |
| $\epsilon_1$                                    | -180.9                          | -146.4                          | -115.0                           | -36.7              | -244.0             |
| $\epsilon_2$                                    | -10.5                           | -10.6                           | -13.3                            | -15.9              | -180.9             |
| $\epsilon_1 + \epsilon_2$                       | -191.4                          | -157.0                          | -128.3                           | -52.6              | -424.9             |
| $E_{\text{Auger}}^c$                            | 52.6                            | 46.7                            | 38.2                             | 507.0              | 2077.6             |
| EOM-CCSD energies                               |                                 |                                 |                                  |                    |                    |
| $E_{\text{IP}}$                                 | 235.0                           | 195.4                           | 159.0                            | 541.4              | 2475.4             |
| $E_{\text{DIP}}$                                | 197.9                           | 162.1                           | 132.3 <sup>e</sup>               | 67.5               | 456.2 <sup>f</sup> |
| $E_{\text{Auger}}^d$                            | 37.1                            | 33.3                            | 26.7                             | 473.9              | 2019.2             |

<sup>a</sup> 2 complex-scaled s, p and d-shells for K-edge decay, 5 complex-scaled s, p, and d-shells for  $L_1$ -edge decay. For details see Sec. III.

<sup>b</sup> Relevant orbitals are  $\phi_{\text{core}} = 2a_1^\beta$  (H<sub>2</sub>S, PH<sub>3</sub>, SiH<sub>4</sub>/L<sub>1</sub>),  $1a_1^\beta$  (H<sub>2</sub>O, H<sub>2</sub>S/K);  $\phi_1 = 1b_1^\beta$  (H<sub>2</sub>S/L<sub>1</sub>),  $3a_1^\beta$  (PH<sub>3</sub>/L<sub>1</sub>),  $1t_2^\beta$  (SiH<sub>4</sub>/L<sub>1</sub>),  $2a_1^\beta$  (H<sub>2</sub>O, H<sub>2</sub>S/K);  $\phi_2 = 2b_1^\alpha$  (H<sub>2</sub>S/L<sub>1</sub>),  $5a_1^\alpha$  (PH<sub>3</sub>/L<sub>1</sub>),  $2t_2^\alpha$  (SiH<sub>4</sub>/L<sub>1</sub>),  $3a_1^\alpha$  (H<sub>2</sub>O, H<sub>2</sub>S/K)

<sup>c</sup> Computed as  $E_{\text{Auger}} = \epsilon_1 + \epsilon_2 - \epsilon_{\text{core}}$ .

<sup>d</sup> Computed as  $E_{\text{Auger}} = E_{\text{IP}} - E_{\text{DIP}}$ .

<sup>e</sup>  $^1A_1$  state resulting from  $1t_2 \otimes 2t_2$ .

<sup>f</sup> Obtained using extrapolation according to Eq. (14).

energies of the doubly ionized states well. As a consequence, it can be expected that CBF-MP2 partial decay widths of  $L_1$ -ionized states evaluated using Eq. (9) are of low quality.

Tab. I demonstrates that using orbital energies from a neutral HF wave function in Eq. (10) leads to qualitatively correct Auger energies. This suggests that CBF-MP2 partial widths can be improved by replacing the orbital energies  $\epsilon_i$ ,  $\epsilon_j$ , and  $\epsilon_{\mathbf{c}}$  in Eq. (9) by those from HF wave functions for the corresponding neutral states, denoted  $\epsilon'$ . This can be written as

$$\gamma_{ij}^{\text{MP2-mod}}(\mathbf{c}) = -2 \text{Im} \left( \sum_a^{n_{\text{virt}}} \frac{\langle a\mathbf{c}||ij\rangle \langle ij||a\mathbf{c}\rangle}{\epsilon_a + \epsilon'_{\mathbf{c}} - \epsilon'_i - \epsilon'_j} \right), \quad (11)$$

which can be viewed as a shift of the MP2 energy denominator.

From Tab. I, it is seen that the energies relevant for K-edge decay of H<sub>2</sub>O and H<sub>2</sub>S are also improved using orbital energies of a neutral HF wave function. However, the effect is less pronounced than for  $L_1$ -edge decay and the use of orbital energies from the core-ionized wave function yields qualitatively correct results. We add that the importance of using qualitatively correct energy differences was already realized in earlier works on Auger decay in which the decay width was evaluated as transition property.<sup>40,82</sup>

### C. Computation of Auger electron energies

In our previous work, we used the EOMDIP-CCSD method<sup>71,72</sup> to compute the energies of the final doubly ionized states. This method is based on applying a linear excitation operator  $\hat{R}^{\text{DIP}}$  to the CCSD wave function,

$$|\Psi_{\text{EOM-CCSD}}\rangle = \hat{R}^{\text{DIP}}|\Psi_{\text{CCSD}}\rangle = \hat{R}^{\text{DIP}}e^{\hat{T}}|\Psi_0\rangle. \quad (12)$$

The operator  $\hat{R}^{\text{DIP}}$  removes two electrons from the wave function and is defined as

$$\hat{R}^{\text{DIP}} = \frac{1}{2} \sum_{ij} r_{ij} j i + \frac{1}{6} \sum_{ijk} \sum_a r_{ijk}^a a^\dagger k j i. \quad (13)$$

The computational cost of the most expensive step in the solution of the EOMDIP-CCSD eigenvalue equations scales as  $\mathcal{O}(n_{\text{occ}}^3 n_{\text{virt}}^3)$  but it requires the preceding solution of the CCSD equations that entail  $\mathcal{O}(n_{\text{occ}}^2 n_{\text{virt}}^4)$  cost. To avoid the latter step, we use the EOM-CCSD(2) approach,<sup>83</sup> also referred to as EOM-MP2, where the CCSD amplitudes are replaced by MP2 amplitudes.

The expressions necessary to solve the EOMDIP-CCSD(2) eigenvalue equations and determine the operator  $\hat{R}^{\text{DIP}}$  are identical to those for EOMDIP-CCSD and also given in the Supporting Information. With this approach, the cost for determining the double ionization energies formally still scales as  $\mathcal{O}(N^6)$ , but since the number of occupied orbitals is much smaller than the number of virtual orbitals in typical complex-variable calculations, the reduction of the operation count from  $\mathcal{O}(n_{\text{occ}}^2 n_{\text{virt}}^4)$  to  $\mathcal{O}(n_{\text{occ}}^3 n_{\text{virt}}^3)$  achieved by skipping the CCSD equations is substantial. Also, the memory requirements are lowered from  $n_{\text{virt}}^4$  to  $n_{\text{virt}}^3 n_{\text{occ}}$  because the EOMDIP equations do not involve integrals  $\langle ab || cd \rangle$ .

With both methods, EOMDIP-CCSD and EOMDIP-CCSD(2), highly correlated states such as those involving holes in the  $2a_1$  orbital are difficult to converge. For such states for which we could not converge the EOMDIP-CCSD or EOMDIP-CCSD(2) eigenvalue equations, the double ionization energies were extrapolated as detailed in the Supporting Information. For this purpose, all double ionization energies were computed with a truncated EOMDIP operator

$$\hat{R}^{\text{DIP, mod}} = \frac{1}{2} \sum_{ij} r_{ij}^{\text{mod}} j i, \quad (14)$$

which only involves 2-hole excitations. A linear relation between the energy in the full excitation manifold and the energy in the reduced excitation manifold was assumed and used to estimate the energy of the states that did not converge in the full excitation manifold.

### D. Construction of Auger spectra

With the partial widths and the Auger electron energies from Sections II A and II C, we construct Auger spectra as follows.<sup>49,50</sup> At the position  $E_K$  corresponding to the transition  $K$  from the core-ionized state with vacant core orbital  $c$  to the doubly ionized state with vacant orbitals  $i$  and  $j$ , a peak

is centered with a broadening that accounts for the measurement uncertainty. In this work, we use Gaussian functions to model the peak shape as

$$I(E) = \sum_{ij} \gamma_{ij}(\mathbf{c}) r_{ij}^2(K) \exp\left[-\frac{4 \ln(2)^2 (E - E_K)^2}{\text{FWHM}}\right] \quad (15)$$

where FWHM is the full-width at half maximum of the Gaussian peak.

Since  $\gamma_{ij}(\mathbf{c})$  and  $E_K$  are obtained from separate calculations, it is necessary to weigh every partial width  $\gamma_{ij}(\mathbf{c})$  by  $r_{ij}(K)$ , which is the amplitude of the excitation  $ji$  in the EOMDIP wave function corresponding to transition  $K$ . This procedure accounts for the change of the wave function during Auger decay.

We note that the extrapolation procedure discussed at the end of Section II C would introduce an imbalance to the spectrum because  $\hat{R}^{\text{DIP, mod}}$  does not include 3-hole-1-particle excitations. Therefore, for every spectrum where the extrapolation procedure was applied, the amplitudes obtained with the full operator  $\hat{R}^{\text{DIP}}$  were renormalized as  $r_{ij}^{2(\text{new})} = r_{ij}^{2(\text{old})} / \sum_{ij} r_{ij}^{2(\text{old})}$  before they were used in Eq. (15).

### III. Computational details

The test set to evaluate the performance of our new CBF-MP2 method for the construction of Auger spectra comprises water, ammonia, methane, hydrogen sulfide, phosphine, and silane. All calculations were performed using a modified version of the Q-Chem program package, version 6.2.<sup>84</sup>

Neutral water, ammonia, and methane all have 10 electrons, while hydrogen sulfide, phosphine, and silane all have 18 electrons. Water and hydrogen sulfide both belong to the  $C_{2v}$  point group, such that the electronic configurations are  $(1a_1)^2(2a_1)^2(1b_2)^2(3a_1)^2(1b_1)^2$  for water and  $(1a_1)^2(2a_1)^2(1b_2)^2(3a_1)^2(1b_1)^2(4a_1)^2(2b_2)^2(5a_1)^2(2b_1)^2$  for hydrogen sulfide. Ammonia and phosphine both belong to the  $C_{3v}$  point group, such that the electronic configurations are  $(1a_1)^2(2a_1)^2(1e)^4(3a_1)^2$  for ammonia and  $(1a_1)^2(2a_1)^2(1e)^4(3a_1)^2(4a_1)^2(2e)^4(5a_1)^2$  for phosphine. Methane and silane both belong to the  $T_d$  point group, such that the electronic configurations are  $(1a_1)^2(2a_1)^2(1t_2)^6$  for methane and  $(1a_1)^2(2a_1)^2(1t_2)^6(3a_1)^2(2t_2)^6$  for silane. The bond lengths and angles used in the calculations can be found in the Supporting Information.

#### A. Basis set details

We use the basis sets that we deemed optimal in our previous works on Auger decay using complex-variable methods.<sup>27,48,49</sup> We start by combining s- and p-shells from the (aug-)cc-pCV5Z basis with d- and f-shells from the (aug-)cc-pCVTZ basis set. While for water, ammonia, and methane, the resulting cc-pCVTZ(5sp) basis set has proven adequate, we employ the augmented version for molecules involving third-row elements.

To these basis sets, several complex-scaled s-, p- and d-shells were added for the CBF-CCSD and CBF-MP2 calculations; the exponents can be found in the Supporting Information. In Sections IV–VI, we denote the addition of  $n$  complex-scaled s-, p-, and d-shells by adding “+ $n(\text{spd})$ ” to the name of

the basis set. EOMDIP-CCSD and EOMDIP-CCSD(2) calculations were carried out in the (aug-)cc-pCVTZ(5sp) basis sets without adding complex-scaled functions.

For O, N, C, and H in calculations on water, ammonia, and methane, the exponents of the complex-scaled shells were taken from ref. 48 where we had determined them by scaling the exponents optimized for the neon atom<sup>27</sup> by factors accounting for the diffuseness of the basis set.

For the calculations on hydrogen sulfide, phosphine, and silane, we first calculated the geometric average of the exponents in the respective aug-cc-pCVTZ (5sp) basis sets. This yielded  $\zeta=5.50, 3.02, 2.57, 2.09,$  and  $0.418$  for Ne, S, P, Si, and H, respectively. We then scaled the optimal exponents for Ne<sup>27</sup> by a factor of  $0.550 = 3.02/5.50, 0.468 = 2.57/5.50, 0.381 = 2.09/5.50,$  and  $0.0762 = 0.418/5.50$  for S, P, Si, and H, respectively, to obtain the exponents for two complex-scaled shells of each angular momentum. In some calculations, one more shell with an exponent between the first two was added to these two shells. In previous work,<sup>51</sup> we found that more than three complex-scaled shells were needed to simultaneously describe  $L_1L_{2,3}M$  Coster-Kronig decay and  $L_1MM$  Auger decay as the emitted electrons have very different energies. Therefore, we add in the present work further complex-scaled shells in an even-tempered manner with a factor of 0.5 starting from the most diffuse of the initial two shells to test the basis-set convergence.

#### IV. K-shell ionization in water, ammonia, and methane

##### A. Core ionization energies and total decay widths

Tab. II shows core ionization energies for water, ammonia, and methane, computed as CCSD or MP2 energy differences between the neutral ground states and the core-ionized states.

TABLE II. Core ionization energies of water, ammonia, and methane computed with CBF-CCSD and CBF-MP2 in the cc-pCVTZ(5sp) basis set with different numbers of complex-scaled s-, p- and d-shells added. All values in eV.

| Method                | H <sub>2</sub> O         | NH <sub>3</sub>      | CH <sub>4</sub>      |
|-----------------------|--------------------------|----------------------|----------------------|
| CBF-CCSD <sup>a</sup> | 539.69                   | 405.56               | 290.83               |
| CBF-MP2 <sup>a</sup>  | 539.94                   | 405.70               | 290.90               |
| CBF-MP2 <sup>b</sup>  | 539.92                   | –                    | –                    |
| expt.                 | 539.73(17) <sup>85</sup> | 405.56 <sup>86</sup> | 290.91 <sup>87</sup> |

<sup>a</sup> 2 complex-scaled s-, p-, and d-shells

<sup>b</sup> 4 complex-scaled s-, p-, and d-shells

The computed energies only differ by 0.07–0.25 eV between the two methods and lie within the experimental error margin. To gauge the convergence of the MP2 results with respect to the number of complex-scaled shells, we conducted an additional calculation for water with 4 instead of 2 complex-scaled s-, p-, and d-shells, which only led to a 0.02 eV decrease in the computed ionization potential.

We point out that the good agreement with experiment is at least partly due to a cancellation of errors: relativistic effects shift the core ionization energies by 0.38 eV (oxygen), 0.21 eV (nitrogen), and 0.10 eV (carbon).<sup>88</sup> When incorporating these values as corrections, the deviation of the present calculations from the experiment amount to up to 0.35 eV.

TABLE III. Total decay widths of core-ionized water, ammonia, and methane computed with CBF-CCSD and CBF-MP2 in the cc-pCVTZ(5sp) basis set with different numbers of complex-scaled s-, p- and d-shells added. All values in meV.

| Method                | $\Gamma$             |                 |                     | $\sum \gamma_{ij}$ |                 |                 |
|-----------------------|----------------------|-----------------|---------------------|--------------------|-----------------|-----------------|
|                       | H <sub>2</sub> O     | NH <sub>3</sub> | CH <sub>4</sub>     | H <sub>2</sub> O   | NH <sub>3</sub> | CH <sub>4</sub> |
| CBF-CCSD <sup>a</sup> | 139.3                | 110.6           | 76.3                | 146.2              | 119.9           | 97.4            |
| CBF-MP2 <sup>a</sup>  | 190.2                | 169.5           | 121.7               | 182.7              | 162.7           | 125.4           |
| CBF-MP2 <sup>b</sup>  | 212.9                | –               | –                   | 209.8              | –               | –               |
| expt.                 | 160(2) <sup>89</sup> |                 | 94(1) <sup>90</sup> |                    |                 |                 |

<sup>a</sup> 2 complex-scaled s-, p-, and d-shells

<sup>b</sup> 4 complex-scaled s-, p-, and d-shells

The total Auger decay widths computed according to Eq. (6) are shown in Tab. III. It is obvious that widths differ more substantially between the methods than energies. MP2 calculations yield widths that are up to 59 meV or 60 % larger than those computed with CCSD, with larger relative deviations for lighter atoms. These deviations are much larger than those observed in EOMIP-CCSD or CIS calculations for the same elements in the same basis set.<sup>48</sup> Furthermore, our previous calculations almost always resulted in narrower decay widths compared to the experimental values, which can be rationalized by the presence of decay processes not accounted for by our model, for example, double Auger decay.<sup>91</sup> On the contrary, the MP2 method yields unphysically high decay widths even though fewer terms are included in the wave function compared to CCSD. The overestimation is only exacerbated by including more complex-scaled shells in the basis.

A measure for the completeness of the basis set in complex-variable calculations for the description of Auger decay is the deviation of the sum of partial widths ( $\sum \gamma_{ij}$ ) from the total width computed with Eq. (6). For the MP2 results in Tab. III, this deviation is 4–8 meV (3–4 %), i.e., somewhat lower than the 7–21 meV (4–8 %) observed for CCSD. However, this lower discrepancy does not mean that either of the two MP2 numbers is a good estimate of the experimental decay width; CCSD results are clearly better.

Notably, the sum of partial widths is always larger than the total width with CCSD, but this is not the case for MP2, where the partial widths add up to lower numbers for water and ammonia. This can be traced back to numerical differences between MP2 and CCSD in the double excitation amplitudes that describe Auger decay.

##### B. Partial decay widths

Partial decay widths for H<sub>2</sub>O, NH<sub>3</sub>, and CH<sub>4</sub> have been computed according to Eqs. (7), (9) and (11). The results for water are presented in Tab. IV, while those for ammonia and methane can be found in the Supporting Information. For some channels, CCSD and MP2 agree within less than 1 meV, whereas large deviations of more than 10 meV occur for other channels. In general, the agreement is better for channels involving the inner-valence 2a<sub>1</sub> orbital than for channels that only involve outer-valence orbitals. For the latter cases, the overestimation can amount to 50% and more, which explains why MP2 yields too large total decay widths (see Tab. III).

TABLE IV. Partial decay widths of core-ionized water computed with CBF-CCSD and CBF-MP2 in the cc-pCVTZ(5sp) basis set with different numbers of complex-scaled s-, p-, and d-shells added. All values in meV.

| Decay channel                              | CCSD   | MP2    |        | MP2-mod |
|--|--------|--------|--------|---------|
|  | +2(sp) | +2(sp) | +4(sp) | +2(sp)  |
| $^1A_1$ (2a <sub>1</sub> 2a <sub>1</sub> ) | 16.7   | 16.4   | 18.8   | 18.7    |
| $^1A_1$ (2a <sub>1</sub> 3a <sub>1</sub> ) | 13.5   | 13.7   | 20.2   | 16.1    |
| $^1B_1$ (2a <sub>1</sub> 1b <sub>1</sub> ) | 12.3   | 12.0   | 19.4   | 18.0    |
| $^1B_2$ (2a <sub>1</sub> 1b <sub>2</sub> ) | 7.3    | 10.0   | 15.5   | 9.9     |
| $^3A_1$ (2a <sub>1</sub> 3a <sub>1</sub> ) | 2.4    | 2.7    | 4.0    | 2.0     |
| $^3B_1$ (2a <sub>1</sub> 1b <sub>1</sub> ) | 2.9    | 2.7    | 4.4    | 2.9     |
| $^3B_2$ (2a <sub>1</sub> 1b <sub>2</sub> ) | 1.9    | 2.1    | 3.2    | 1.5     |
| $^1A_1$ (3a <sub>1</sub> 3a <sub>1</sub> ) | 11.7   | 17.4   | 18.4   | 11.2    |
| $^1A_1$ (1b <sub>1</sub> 1b <sub>1</sub> ) | 16.5   | 23.6   | 23.4   | 15.5    |
| $^1A_1$ (1b <sub>2</sub> 1b <sub>2</sub> ) | 10.1   | 13.9   | 12.9   | 9.0     |
| $^1B_1$ (3a <sub>1</sub> 1b <sub>1</sub> ) | 16.4   | 25.4   | 27.6   | 16.1    |
| $^1B_2$ (3a <sub>1</sub> 1b <sub>2</sub> ) | 17.5   | 20.8   | 18.4   | 14.5    |
| $^1A_2$ (1b <sub>1</sub> 1b <sub>2</sub> ) | 14.2   | 21.7   | 23.1   | 12.8    |
| $^3B_1$ (3a <sub>1</sub> 1b <sub>1</sub> ) | 0.3    | 0.2    | 0.3    | 0.2     |
| $^3B_2$ (3a <sub>1</sub> 1b <sub>2</sub> ) | 0.2    | 0.2    | 0.2    | 0.1     |
| $^3A_2$ (1b <sub>1</sub> 1b <sub>2</sub> ) | 0.0    | 0.0    | 0.0    | 0.0     |
| Sum  | 146.2  | 182.7  | 209.8  | 148.5   |

Notably, increasing the size of the basis set for the MP2 calculation leads to an even larger disagreement and channels involving inner-valence orbitals start to be affected as well. For triplet channels, deviations between CCSD and MP2 are lower than for singlet channels but this has little impact because triplet channels have low intensities anyhow.

For water, we also computed partial widths according to Eq. (11). As expected, these MP2-mod results are in better agreement with CCSD for most channels. Especially those channels whose intensities are overestimated by regular MP2 have lower width and the sum of partial widths differs from the CCSD result by no more than 2 meV. The root mean square (RMS) deviation with respect to CCSD decreases from 4 meV to 2 meV. However, there are some decay channels, e.g.,  $^1B_1$  (2a<sub>1</sub>1b<sub>1</sub>) (third line in Tab. IV) for which MP2-mod deviates substantially from CCSD.

### C. Auger spectra

To construct Auger spectra, we computed the energies of the doubly ionized states with the EOMDIP-CCSD(2) and EOMDIP-CCSD methods. These results are reported in the Supporting Information and in excellent agreement for all molecules, as exemplified for water in Table V. In this case, the maximum deviation between the methods water amounts to 0.18 eV and the RMS deviation to 0.08 eV. Similar to the partial decay widths, deviations are lower for higher-lying states, i.e., those with holes in inner-valence orbitals.

The resulting Auger spectra are shown in Fig. 1. For water and methane, our spectra are shifted by 1.7 eV and 1.5 eV, respectively, to higher energies so that the highest-energy peak coincides with the experimental spectrum. The FWHM is 2.0 eV for water and 1.5 eV for ammonia and methane. Consistent with the small deviations between EOMDIP-CCSD and EOMDIP-CCSD(2) for the double ionization energies, the

TABLE V. Lowest double ionization energies of water in eV computed with EOMDIP-CCSD and EOMDIP-CCSD(2) in the cc-pCVTZ(5sp) basis set.

| Electronic state | Leading amplitude               | Double ionization energies |                |
|------------------|---------------------------------|----------------------------|----------------|
|                  |                                 | EOMDIP-CCSD                | EOMDIP-CCSD(2) |
| $^3B_1$          | 3a <sub>1</sub> 1b <sub>1</sub> | 41.01                      | 41.15          |
| $^1A_1$          | 1b <sub>1</sub> 1b <sub>1</sub> | 42.04                      | 42.22          |
| $^1B_1$          | 3a <sub>1</sub> 1b <sub>1</sub> | 43.44                      | 43.58          |
| $^3A_2$          | 1b <sub>1</sub> 1b <sub>2</sub> | 45.08                      | 45.15          |
| $^1A_1$          | 3a <sub>1</sub> 3a <sub>1</sub> | 46.48                      | 46.58          |
| $^1A_2$          | 1b <sub>1</sub> 1b <sub>2</sub> | 46.84                      | 46.92          |
| $^3B_2$          | 3a <sub>1</sub> 1b <sub>2</sub> | 46.90                      | 46.93          |
| $^1B_2$          | 3a <sub>1</sub> 1b <sub>2</sub> | 48.99                      | 49.03          |
| $^1A_1$          | 1b <sub>2</sub> 1b <sub>2</sub> | 53.79                      | 53.81          |
| $^3B_1$          | 2a <sub>1</sub> 1b <sub>1</sub> | 59.54                      | 59.62          |
| $^3A_1$          | 2a <sub>1</sub> 3a <sub>1</sub> | 61.25                      | 61.29          |
| $^3B_2$          | 2a <sub>1</sub> 1b <sub>2</sub> | 65.20                      | 65.19          |
| $^1B_1$          | 2a <sub>1</sub> 1b <sub>1</sub> | 66.25                      | 66.33          |
| $^1A_1$          | 2a <sub>1</sub> 3a <sub>1</sub> | 67.49                      | 67.56          |
| $^1B_2$          | 2a <sub>1</sub> 1b <sub>2</sub> | 72.45                      | 72.45          |
| $^1A_1$          | 2a <sub>1</sub> 2a <sub>1</sub> | 85.90                      | 85.88          |

peak positions of our theoretical spectra are in excellent agreement for each molecule. For water, we also show restricted active space second-order perturbation theory (RASPT2) and multireference configuration interaction (MRCI) spectra,<sup>33,47</sup> whose peak positions are in good agreement with ours.

We normalized all spectra such that the most intense peak in every spectrum has the same height. This explains why the agreement between CBF-CCSD and CBF-MP2 is better at high Auger electron energies, even though the partial widths in Tab. IV deviate more for channels corresponding to low Auger electron energies.

In general, the intensity distribution of our spectra matches the experimental spectra well: all peaks and shoulders in the experiments can be assigned unequivocally. However, for water both CBF-CCSD and CBF-MP2 assign less intensity to the peak with the highest Auger electron energy than to the next peak, whereas the opposite pattern was found in the experiment. For ammonia, there is no such disagreement, while the two respective peaks coalesce for methane.

The origin of the disagreement in the spectrum of water becomes clear by looking at previous theoretical studies. While a different approach for the continuum improves the peak intensities only to a certain degree as shown in Ref. 47, the consideration of nuclear motion via ab initio molecular dynamics (AIMD) as done in Ref. 33 (light blue line in Fig. 1) resolves most of the disagreement with the experiment, both at high energies and low energies. We note that the consideration of vibrational effects does not necessarily require an AIMD approach. In fact, the impact of vibrational broadening on the peak shapes can be captured using a simplified model<sup>95</sup> that can be combined easily with complex-variable techniques.<sup>74</sup>

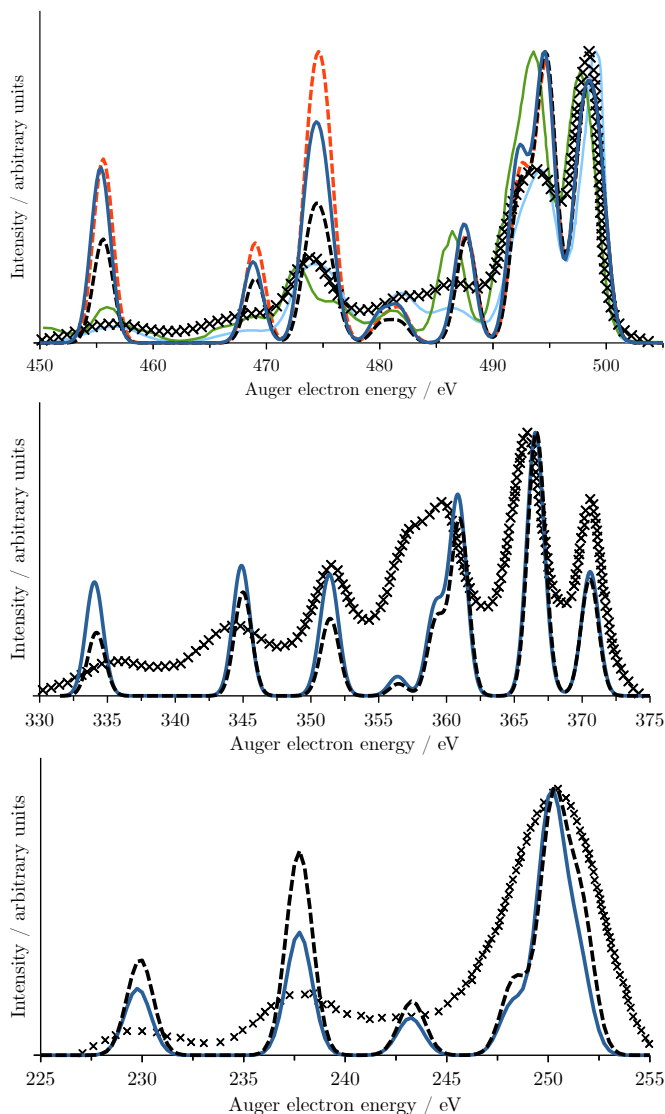


FIG. 1. Auger spectra of water (top), ammonia (middle), and methane (bottom). Dark blue full line: CBF-CCSD/EOMDIP-CCSD, black dashed line: CBF-MP2/EOMDIP-CCSD(2), orange dashed line: CBF-MP2-mod/EOMDIP-CCSD(2), green line: RASPT2/one-center approximation,<sup>47</sup> light blue line: MRCI/single-center expansion,<sup>33</sup> black  $\times$ : experiment.<sup>92–94</sup>

## V. K-shell ionization in hydrogen sulfide, phosphine, and silane

### A. Core ionization energies and total decay widths

K-edge core ionization energies for hydrogen sulfide, phosphine, and silane are presented in Tab. VI. Compared to the lighter molecules ( $\text{H}_2\text{O}$ ,  $\text{NH}_3$ ,  $\text{CH}_4$ ), our results for  $\text{H}_2\text{S}$ ,  $\text{PH}_3$ , and  $\text{SiH}_4$  deviate more from the experimental values. The computed values are several eV lower, which can be attributed to scalar relativistic effects.<sup>96</sup> However, CBF-CCSD and CBF-MP2 agree with each other to the same degree as for the lighter molecules (0.13–0.22 eV). Similar to water (Tab. II), increasing the number of complex-scaled shells has a negligible effect on the core ionization energy of  $\text{H}_2\text{S}$ .

TABLE VI. K-edge core ionization energies of hydrogen sulfide, phosphine, and silane computed with CBF-CCSD and CBF-MP2 in the aug-cc-pCVTZ(5sp) basis set with different numbers of complex scaled s-, p- and d-shells added. All values in eV.

| Method                | $\text{H}_2\text{S}$  | $\text{PH}_3$ | $\text{SiH}_4$     |
|-----------------------|-----------------------|---------------|--------------------|
| CBF-CCSD <sup>a</sup> | 2472.05               | 2146.20       | 1843.71            |
| CBF-MP2 <sup>a</sup>  | 2472.18               | 2146.40       | 1843.93            |
| CBF-MP2 <sup>b</sup>  | 2472.28               | —             | —                  |
| expt.                 | 2478.25 <sup>97</sup> | —             | 1847 <sup>98</sup> |

<sup>a</sup> 2 complex-scaled s-, p-, and d-shells

<sup>b</sup> 4 complex-scaled s-, p-, and d-shells

TABLE VII. Total decay widths of K-edge core-ionized hydrogen sulfide, phosphine, and silane computed with CBF-CCSD and CBF-MP2 in the aug-cc-pCVTZ(5sp) basis set with different numbers of complex scaled s-, p- and d-shells added. All values in meV.

| Method                | $\Gamma$               |               |                | $\sum \gamma_{ij}$   |               |                |
|-----------------------|------------------------|---------------|----------------|----------------------|---------------|----------------|
|                       | $\text{H}_2\text{S}$   | $\text{PH}_3$ | $\text{SiH}_4$ | $\text{H}_2\text{S}$ | $\text{PH}_3$ | $\text{SiH}_4$ |
| CBF-CCSD <sup>a</sup> | 443.6                  | 423.1         | 343.8          | 446.6                | 416.9         | 386.1          |
| CBF-MP2 <sup>a</sup>  | 484.1                  | 452.0         | 409.7          | 448.1                | 435.6         | 428.8          |
| CBF-MP2 <sup>b</sup>  | 495.7                  | —             | —              | 494.9                | —             | —              |
| expt.                 | 500(100) <sup>97</sup> | —             | —              | —                    | —             | —              |

<sup>a</sup> 2 complex-scaled s-, p-, and d-shells

<sup>b</sup> 4 complex-scaled s-, p-, and d-shells

Total decay widths are presented in Tab. VII. They are up to 4 times larger for hydrogen sulfide, phosphine, and silane than for water, ammonia, and methane and increase with the charge of the central atom, which complies with the expected trend.<sup>8,99</sup> For hydrogen sulfide, an experimental value is available,<sup>97</sup> which agrees with our results taking into account the measurement uncertainty.

The MP2 total decay widths are 30–70 meV larger than the CCSD values, which is a similar absolute deviation as for the second-row compounds (Tab. III). However, it represents a much lower relative deviation. Comparing the sum of partial widths with the total width, good agreement is only observed for CCSD calculations on  $\text{H}_2\text{S}$  and  $\text{PH}_3$  but not for any MP2 calculation. For the MP2 calculation on  $\text{H}_2\text{S}$ , the addition of more complex-scaled shells brings the sum of partial widths closer to the total width.

### B. Partial decay widths

Partial widths for  $\text{H}_2\text{S}$ ,  $\text{PH}_3$ , and  $\text{SiH}_4$ , summarized by the involved shells, are presented in Tab. VIII. In addition to the absolute values, Tab. VIII shows the relative distribution among the channels in percent as well as a hypothetical distribution based on the assumption that all channels have the same width. For  $\text{H}_2\text{S}$ , we conducted additional calculations with 4 instead of 2 complex-scaled s-, p-, and d-shells; these results can be found in the Supporting Information. The basis-set dependence of these CBF-MP2 widths is much less pronounced than for water (Tab. IV).

For all molecules, singlet decay channels account for ca. 95% of the decay width, which matches the expectation for K-edge Auger spectra.<sup>44,48,52,100</sup> Also, the largest share of the decay width (89–94%) stems from LL channels, while

TABLE VIII. Branching ratios for Auger decay of K-edge core-ionized H<sub>2</sub>S, PH<sub>3</sub>, and SiH<sub>4</sub> computed with CBF-CCSD and CBF-MP2 in the aug-cc-pCVTZ(5sp)+2(sp) basis.

| Branch                            | $\Sigma \gamma_j / \text{meV}$ |                 |                  |                  |                 |                  | $\Sigma \gamma_j / \Gamma / \%$ |                 |                  |                  |                 |                  | Same width<br>for every<br>channel / % |
|-----------------------------------|--------------------------------|-----------------|------------------|------------------|-----------------|------------------|---------------------------------|-----------------|------------------|------------------|-----------------|------------------|--|
|                                   | CCSD                           |                 |                  | MP2              |                 |                  | CCSD                            |                 |                  | MP2              |                 |                  |  |
|                                   | H <sub>2</sub> S               | PH <sub>3</sub> | SiH <sub>4</sub> | H <sub>2</sub> S | PH <sub>3</sub> | SiH <sub>4</sub> | H <sub>2</sub> S                | PH <sub>3</sub> | SiH <sub>4</sub> | H <sub>2</sub> S | PH <sub>3</sub> | SiH <sub>4</sub> |  |
| L <sub>1</sub> L <sub>1</sub>     | 24.6                           | 23.4            | 22.8             | 25.8             | 25.0            | 19.8             | 5.5                             | 5.6             | 5.9              | 4.9              | 5.7             | 4.6              | 1.6                                    |
| L <sub>1</sub> L <sub>2,3</sub>   | 125.4                          | 119.5           | 111.4            | 127.8            | 124.5           | 119.9            | 28.1                            | 28.7            | 28.8             | 27.0             | 28.6            | 28.0             | 9.4                                    |
| L <sub>1</sub> M <sub>1</sub>     | 4.4                            | 3.7             | 3.3              | 5.0              | 4.3             | 2.8              | 1.0                             | 0.9             | 0.9              | 0.6              | 1.0             | 0.7              | 3.1                                    |
| L <sub>1</sub> M <sub>2,3</sub>   | 7.6                            | 5.5             | 3.5              | 7.6              | 5.7             | 3.5              | 1.7                             | 1.3             | 0.9              | 1.7              | 1.3             | 0.8              | 9.4                                    |
| L <sub>2,3</sub> L <sub>2,3</sub> | 249.6                          | 239.1           | 227.0            | 247.2            | 249.5           | 262.9            | 55.9                            | 57.4            | 58.8             | 57.1             | 57.3            | 61.3             | 14.1                                   |
| L <sub>2,3</sub> M <sub>1</sub>   | 8.2                            | 6.5             | 5.1              | 8.2              | 6.8             | 5.3              | 1.8                             | 1.6             | 1.3              | 1.9              | 1.6             | 1.2              | 9.4                                    |
| L <sub>2,3</sub> M <sub>2,3</sub> | 25.6                           | 18.4            | 12.6             | 24.8             | 18.8            | 14.0             | 5.7                             | 4.4             | 3.3              | 6.4              | 4.3             | 3.3              | 28.1                                   |
| M <sub>1</sub> M <sub>1</sub>     | 0.2                            | 0.2             | 0.1              | 0.2              | 0.2             | 0.1              | 0.1                             | 0.0             | 0.0              | 0.0              | 0.1             | 0.0              | 1.6                                    |
| M <sub>1</sub> M <sub>2,3</sub>   | 0.4                            | 0.3             | 0.1              | 0.6              | 0.4             | 0.2              | 0.1                             | 0.1             | 0.0              | 0.1              | 0.1             | 0.0              | 9.4                                    |
| M <sub>2,3</sub> M <sub>2,3</sub> | 0.6                            | 0.3             | 0.2              | 0.6              | 0.4             | 0.2              | 0.1                             | 0.1             | 0.0              | 0.2              | 0.1             | 0.0              | 14.1                                   |
| LL                                | 399.6                          | 382.0           | 361.1            | 400.8            | 399.0           | 402.6            | 89.5                            | 91.6            | 93.5             | 89.0             | 91.6            | 93.9             | 25                                     |
| LM                                | 45.8                           | 34.1            | 24.5             | 45.6             | 35.7            | 25.7             | 10.2                            | 8.2             | 6.4              | 10.6             | 8.2             | 6.0              | 50                                     |
| MM                                | 1.2                            | 0.8             | 0.4              | 1.4              | 0.9             | 0.5              | 0.3                             | 0.2             | 0.1              | 0.3              | 0.2             | 0.1              | 25                                     |

LM channels account for 6–11% and the contribution of MM channels remains below 1%. Thus, assuming equal widths for all singlet channels, which is an acceptable approximation for Auger decay of second-row elements,<sup>49,50,101</sup> is not applicable in the third row of the periodic table.

The dominance of the LL channels can be related to the energetic and spatial proximity of the L shell to the initial hole in the K shell. We also note that LL channels contribute somewhat more intensity for SiH<sub>4</sub> than for PH<sub>3</sub> and H<sub>2</sub>S. In line with the low intensity of the LM and MM channels, no measurements of KLM or KMM Auger spectra of H<sub>2</sub>S, PH<sub>3</sub>, and SiH<sub>4</sub> have been reported. Within the KLL branch, more than half of the intensity stems from L<sub>2,3</sub>L<sub>2,3</sub> channels, i.e., channels involving two 2p-like orbitals. Their dominance is more pronounced for SiH<sub>4</sub> than for PH<sub>3</sub> and H<sub>2</sub>S, which is in line with experimental results.<sup>102</sup> Also, we found the same trend for second-row elements in our previous work.<sup>48</sup>

As is evident from Tab. VIII, CBF-CCSD and CBF-MP2 predict almost identical KLL:KLM:KMM branching ratios. More substantial deviations are observed for the KL<sub>1</sub>L<sub>1</sub>:KL<sub>2,3</sub>L<sub>2,3</sub> branching ratios, especially for SiH<sub>4</sub>. This can be traced back to the overestimation of the widths involving the 2p orbitals by CBF-MP2. For the widths of individual channels, the RMS deviation between CBF-CCSD and CBF-MP2 amounts to only 0.5 meV. In view of this good agreement, we did not conduct MP2-mod calculations according to Eq. (11).

The largest individual partial widths for hydrogen sulfide are shown in Tab. IX. The remaining data are available from the Supporting Information. There are several groups of three channels with very similar widths, for example the three strongest channels <sup>1</sup>B<sub>2</sub> (3a<sub>1</sub>1b<sub>2</sub>), <sup>1</sup>B<sub>1</sub> (3a<sub>1</sub>1b<sub>1</sub>), and <sup>1</sup>A<sub>2</sub> (1b<sub>1</sub>1b<sub>2</sub>). This similarity is a consequence of the atom-like character of the 2p orbitals. In an atom, these orbitals would be degenerate and the partial widths would be identical, disregarding spin-orbit effects.<sup>103</sup>

The small impact of the hydrogen atoms on the 2p orbitals of sulfur in H<sub>2</sub>S also becomes clear by comparing decay widths between H<sub>2</sub>S and H<sub>2</sub>O. This comparison is shown

TABLE IX. Largest partial decay widths of hydrogen sulfide in meV computed with CBF-CCSD and CBF-MP2 in the aug-cc-pCVTZ(5sp)+2(sp) basis.

| Decay channel  | $\gamma_j$ |      |
|--|------------|------|
|  | CCSD       | MP2  |
| <sup>1</sup> B <sub>2</sub> (3a <sub>1</sub> 1b <sub>2</sub> ) | 47.8       | 46.2 |
| <sup>1</sup> B <sub>1</sub> (3a <sub>1</sub> 1b <sub>1</sub> ) | 47.0       | 45.4 |
| <sup>1</sup> A <sub>2</sub> (1b <sub>1</sub> 1b <sub>2</sub> ) | 46.9       | 45.3 |
| <sup>1</sup> A <sub>1</sub> (1b <sub>1</sub> 1b <sub>1</sub> ) | 36.6       | 37.8 |
| <sup>1</sup> A <sub>1</sub> (3a <sub>1</sub> 3a <sub>1</sub> ) | 35.7       | 36.3 |
| <sup>1</sup> A <sub>1</sub> (1b <sub>2</sub> 1b <sub>2</sub> ) | 35.5       | 36.1 |
| <sup>1</sup> B <sub>1</sub> (2a <sub>1</sub> 1b <sub>1</sub> ) | 35.4       | 35.9 |
| <sup>1</sup> A <sub>1</sub> (2a <sub>1</sub> 3a <sub>1</sub> ) | 35.3       | 35.8 |
| <sup>1</sup> B <sub>2</sub> (2a <sub>1</sub> 1b <sub>2</sub> ) | 35.3       | 35.8 |
| <sup>1</sup> A <sub>1</sub> (2a <sub>1</sub> 2a <sub>1</sub> ) | 24.6       | 25.9 |
| <sup>3</sup> B <sub>1</sub> (2a <sub>1</sub> 1b <sub>1</sub> ) | 6.5        | 6.8  |

in the Supporting Information. For both molecules, the most intense channel is <sup>1</sup>B<sub>2</sub> (3a<sub>1</sub>1b<sub>1</sub>), but there are significant variations among the remaining channels. The groups of three channels that have almost the same width for H<sub>2</sub>S have different widths for H<sub>2</sub>O. Also, the <sup>1</sup>A<sub>1</sub> (2a<sub>1</sub>2a<sub>1</sub>) channel has a higher relative intensity in water than in hydrogen sulfide.

### C. KLL Auger spectra

To construct Auger spectra, we computed double ionization energies of H<sub>2</sub>S, PH<sub>3</sub>, and SiH<sub>4</sub> with EOMDIP-CCSD and EOMDIP-CCSD(2). Similar to H<sub>2</sub>O, NH<sub>3</sub>, and CH<sub>4</sub>, the deviations between the methods are relatively low. For example, for hydrogen sulfide, the maximum deviation is 0.50 eV and the RMS deviation is 0.38 eV. For LL states, the RMS deviation is somewhat higher (0.55 eV) than for LM states (0.25 eV) and MM states (0.12 eV). This can be rationalized considering that the LL double ionization energies are an order of magnitude larger than those of MM states. For LL and LM states, EOMDIP-CCSD(2) yields higher double ionization energies than EOMDIP-CCSD, while it yields lower values for MM states.

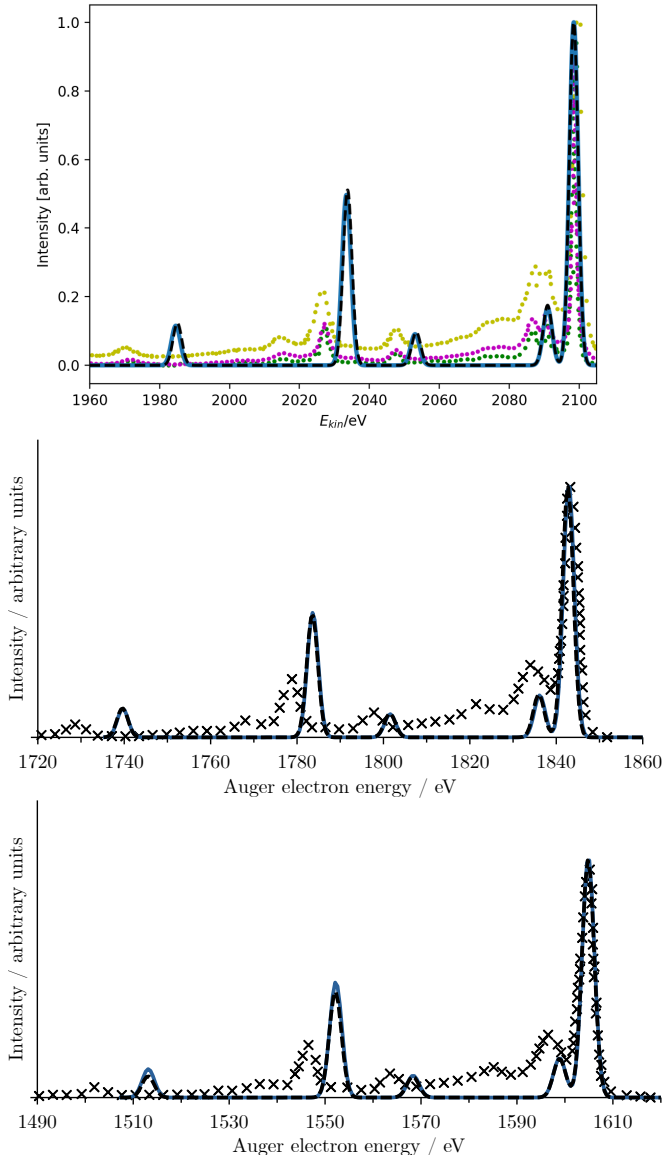


FIG. 2. KLL Auger spectra of hydrogen sulfide (top), phosphine (middle), and silane (bottom). Dark blue full line: CBF-CCSD/EOMDIP-CCSD, black dashed line: CBF-MP2/EOMDIP-CCSD(2), green dots: experiment (ref. 104), yellow dots: experiment (ref. 105), purple dots: experiment (ref. 106), black  $\times$ : experiment (ref. 102).

The resulting KLL Auger spectra are shown in Fig. 2 together with the corresponding experimental spectra.<sup>102,104–106</sup> Our computed spectra are shifted to higher energies by 18.35, 17.25, and 17.25 eV (MP2) and 17.85, 17.10, and 17.10 eV (CCSD) for H<sub>2</sub>S, PH<sub>3</sub>, and SiH<sub>4</sub>, respectively, so that the highest-energy peak coincides with the experimental spectrum. The FWHM is 3.0 eV for all spectra. The intensities of the peaks are normalized such that the highest peaks have the same intensity.

The KLL branch is the only part of the spectra that has been

measured. The spectra of H<sub>2</sub>S, PH<sub>3</sub>, and SiH<sub>4</sub> resemble each other closely; 7 (PH<sub>3</sub>, SiH<sub>4</sub>) and 8 (H<sub>2</sub>S) peaks can be identified in them. Our computed CBF-CCSD and CBF-MP2 spectra are practically indistinguishable from each other for every molecule and only include 5 peaks. The lowest-energy peak corresponds to the L<sub>1</sub>L<sub>1</sub> (2a<sub>1</sub>2a<sub>1</sub>) decay channel. The second peak is formed by the three singlet L<sub>1</sub>L<sub>2,3</sub> states, while the corresponding triplet states form the third peak. The fourth peak corresponds to a totally symmetric <sup>1</sup>A<sub>1</sub> transition and belongs to the L<sub>2,3</sub>L<sub>2,3</sub> branch. The highest-energy peak of the KLL spectrum is formed by five quasi-degenerate L<sub>2,3</sub>L<sub>2,3</sub> channels.

Compared to the experiment, one observes that the lower-energy signals in our computed spectra are shifted to higher energies for all molecules: the L<sub>1</sub>L<sub>1</sub> feature by about 14 eV and the L<sub>1</sub>L<sub>2,3</sub> signals by about 7 eV. The likely reason is the use of the truncated EOMDIP operator [Eq. (14)] and the subsequent extrapolation procedure specified in Sec II C for the computation of the double ionization energies corresponding to these channels.

The main disagreement in the peak intensity between experiment and theory is that we overestimate the two peaks at lower kinetic energy compared to the three highest-energy peaks. We observed a similar overestimation in our previous work<sup>49</sup> and could remedy it by taking into account the extent of 3-hole-1-particle excitations in the EOMDIP-CCSD wavefunction. In the present case, however, this is not possible as the doubly ionized states in question could be only computed with the truncated operator from Eq. (14).

Also, all experimental spectra have two peaks that are absent in the computed spectra: one of them is located at 2015 eV (H<sub>2</sub>S), 1768 eV (PH<sub>3</sub>), 1537 eV (SiH<sub>4</sub>), while the other one is observed at 2075 eV (H<sub>2</sub>S), 1822 eV (PH<sub>3</sub>), 1585 eV (SiH<sub>4</sub>). The nature of these peaks remains unclear, a possible origin could be shake-up or shake-off transitions, which are not included in our model. Also, our computed spectra do not account for spin-orbit coupling,<sup>103</sup> which may be responsible for the splitting of the peak at 2087 eV in the H<sub>2</sub>S spectrum.

Comparing H<sub>2</sub>S, PH<sub>3</sub> and SiH<sub>4</sub> with H<sub>2</sub>O, NH<sub>3</sub> and CH<sub>4</sub>, one sees that the spectra of the latter molecules span a range of at most 50 eV, while those of the former extend over up to 120 eV. This illustrates the larger separation of the orbital energies in the third-row hydrides, which is a consequence of the larger ionization energies and ultimately the larger nuclear charges. Another difference is the lower number of distinct signals in the spectra of the third-row hydrides. This is because the atom-like character of the L-shell orbitals renders them almost degenerate; the respective decay channels have very similar energies. In second-row hydrides, the L-shell orbitals are involved in bonding and have different energies depending on their orientation relative to the hydrogen atoms.

#### D. KLM Auger spectra

Our computed KLM Auger spectra for H<sub>2</sub>S are shown in Fig. 3. They are shifted by 18.35 eV (MP2) and 17.85 eV (CCSD), respectively, to higher energies to match the shifts applied in Fig. 2. The FWHM is 1.5 eV for both spectra.

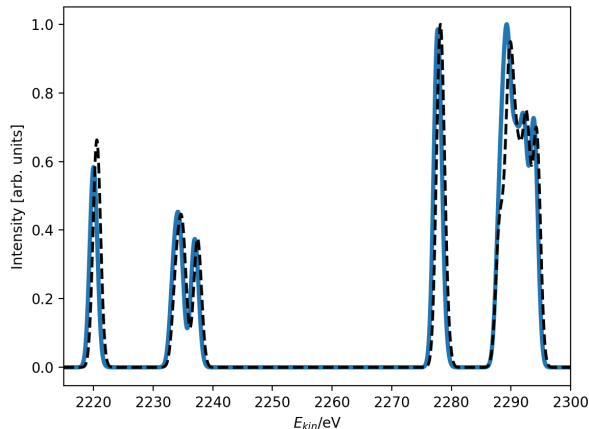


FIG. 3. KLM Auger spectrum of hydrogen sulfide. Dark blue full line: CBF-CCSD/EOMDIP-CCSD, dashed black line: CBF-MP2/EOMDIP-CCSD(2).

The KLM spectrum possesses a similar number of features as the KLL spectrum. 7 signals are distinguishable and grouped into two features that are separated by a 40 eV gap, which reflects the splitting between the  $L_1$  and the  $L_{2,3}$  orbitals. The higher-energy feature comprises 3 peaks at 2292 eV, which are so close to each other that they coalesce to a broader signal, and an isolated peak at 2278 eV. The 14 eV gap between these two signals corresponds to the energy difference between the  $M_1$  and  $M_{2,3}$  orbitals. The lower-energy feature comprises 2 peaks around 2237 eV and an isolated peak at 2220 eV. The gap between these signals again corresponds to the energy difference between the  $M_1$  and  $M_{2,3}$  orbitals.

The peak positions differ slightly between our two KLM spectra because the double ionization energies were shifted for each method separately to align the most intensive peak in the KLL spectrum. However, it is evident that this only leads to local shifts specific to a particular spectral region. The peak intensities are in good agreement, with lower-energy signals slightly overestimated by CBF-MP2. This is opposite to water, where the higher-energy signals were severely overestimated by CBF-MP2.

## VI. L-shell core ionization

### A. Core ionization energies and total decay widths

$L_1$ -edge core ionization energies for hydrogen sulfide, phosphine, and silane are reported in Tab. X. We used EOMIP-CCSD as reference method because the CCSD equations could not be converged for these states, neither in a complex-scaled basis set nor an entirely real-valued basis set. Although it is no problem to construct the respective HF wave functions and compute the MP2 energy using Eq. (8), the large norms of the MP2 amplitudes [for example,  $36 - 16i$  for  $H_2S(2a_1^{-1})$  as compared to  $0.33 - 0.0007i$  for  $H_2S(1a_1^{-1})$ ], both computed in the aug-cc-pCVTZ (5sp) + 4(spd) basis] show that the description is of low quality.

TABLE X.  $L_1$ -edge ionization energies of  $H_2S$ ,  $PH_3$ , and  $SiH_4$  computed with CBF-MP2 and CBF-EOMIP-CCSD in the aug-cc-pCVTZ(5sp) basis with different numbers of complex-scaled s-, p-, and d-shells added. All values in eV.

| Method                  | CBFs    | $H_2S$                       | $PH_3$                | $SiH_4$            |
|-------------------------|---------|------------------------------|-----------------------|--------------------|
| MP2                     | +4(spd) | 223.78                       | 193.01                | 155.87             |
| MP2                     | +5(spd) | 219.53                       | 192.99                | 155.86             |
| MP2                     | +6(spd) | 229.08                       | 192.96                | 155.86             |
| MP2                     | +8(spd) | 233.96                       | –                     | –                  |
| EOMIP-CCSD <sup>a</sup> | +6(spd) | 234.98                       | 195.36                | 159.04             |
| EOMIP-CCSD <sup>a</sup> | +8(spd) | 234.99                       | –                     | –                  |
| Experiment              |         | $235.0 \pm 0.1$ <sup>b</sup> | $194.88$ <sup>c</sup> | $155$ <sup>d</sup> |

<sup>a</sup> EOMIP-CCSD results for  $H_2S$  were taken from Ref. 51.

<sup>b</sup> From Ref. 107

<sup>c</sup> From Ref. 108

<sup>d</sup> From Ref. 109

Indeed, the MP2  $L_1$ -edge ionization energies in Tab. X deviate substantially from EOMIP-CCSD, while we observed a good match between MP2 and CCSD for K-edge ionization energies in Tabs. II and VI. In addition, the MP2 energy shows a rather erratic dependence on the complex-scaled part of the basis set for  $H_2S$ .

EOMIP-CCSD agrees with experimental  $L_1$ -edge ionization energies of  $H_2S$  and  $PH_3$  within less than 0.5 eV. For  $SiH_4$ , there is a deviation of 4 eV, but the experimental value was reported as “approximate”.<sup>109</sup>

The total decay widths of the  $L_1$ -edge ionized states are reported in Tab. XI. These states can undergo  $L_1L_{2,3}M$  Coster-Kronig decay where an electron from the  $L_{2,3}$ -shell fills the vacancy in the  $L_1$ -shell and, therefore, have considerably larger decay widths than K-edge ionized states.<sup>110</sup> This is illustrated by the EOMIP-CCSD results in Tab. XI. For  $H_2S$ , our EOMIP-CCSD decay width is in good agreement with the experimental value,<sup>107</sup> while no experimental decay widths are available for  $PH_3$  and  $SiH_4$ .

Comparing the sum of EOMIP-CCSD partial widths to the total decay width, a larger deviation is observed for the  $L_1$ -edge ionized states in Tab. XI than for K-edge ionized states (Tabs. III and VII). Also, more complex-scaled shells are needed to describe Coster-Kronig decay than Auger decay of K-edge ionized states. For a further discussion of these aspects, we refer to our previous work on hydrogen sulfide and argon.<sup>51</sup>

As can be expected from the analysis in Sec. II B, the decay widths computed with MP2 are completely wrong. For  $H_2S$ , an erratic dependence on the complex-scaled part of the basis set is observed. For  $PH_3$  and  $SiH_4$ , results are stable with respect to the basis set, but too low by more than a factor of 20. The severe underestimation of the widths of  $PH_3$  and  $SiH_4$  can be understood based on Tab. I: According to the orbital energies of the  $L_1$ -edge ionized HF wave functions, the Coster-Kronig  $L_{2,3}M$  decay channels are closed. The widths in Tab. XI thus represent only the contribution of the MM decay channels, which in reality account for less than 5%.

To assess the validity of the “modified” MP2 method from Sec. II B, we recomputed all decay widths using Eq. (11). The sums of the respective decay widths still deviate by up

TABLE XI. Total decay widths of  $L_1$ -edge ionized  $H_2S$ ,  $PH_3$ , and  $SiH_4$  computed with CBF-MP2 and CBF-EOMIP-CCSD in the aug-cc-pCVTZ(5sp) basis with different numbers of complex-scaled  $s$ -,  $p$ -, and  $d$ -shells added. All values in meV.

| Method                  | CBFs         | $H_2S$   |                    | $PH_3$   |                    | $SiH_4$  |                    |
|-------------------------|--------------|----------|--------------------|----------|--------------------|----------|--------------------|
|                         |              | $\Gamma$ | $\sum \gamma_{ij}$ | $\Gamma$ | $\sum \gamma_{ij}$ | $\Gamma$ | $\sum \gamma_{ij}$ |
| MP2                     | +2(sp $d$ )  | 526.3    | 522.2              | 51.3     | 45.2               | 18.9     | 15.1               |
| MP2                     | +4(sp $d$ )  | 3493.9   | 3420.1             | 48.1     | 69.9               | 25.5     | 30.6               |
| MP2                     | +5(sp $d$ )  | 19505.7  | 19524.8            | 77.4     | 94.5               | 26.6     | 37.2               |
| MP2                     | +6(sp $d$ )  | 3708.0   | 3833.1             | 59.0     | 77.8               | 27.8     | 41.1               |
| MP2                     | +8(sp $d$ )  | 1723.4   | 1914.7             | –        | –                  | –        | –                  |
| MP2                     | +10(sp $d$ ) | 99.8     | 106.3              | –        | –                  | –        | –                  |
| MP2-mod                 | +5(sp $d$ )  | –        | 2063.6             | –        | 1676.3             | –        | 1500.2             |
| MP2-mod                 | +8(sp $d$ )  | –        | 2157.5             | –        | –                  | –        | –                  |
| EOMIP-CCSD <sup>a</sup> | +4(sp $d$ )  | 1119.1   | 1020.0             | –        | –                  | –        | –                  |
| EOMIP-CCSD <sup>a</sup> | +6(sp $d$ )  | 1603.2   | 1407.4             | 1287.1   | –                  | 1017.8   | –                  |
| EOMIP-CCSD <sup>a</sup> | +8(sp $d$ )  | 1672.2   | 1440.5             | –        | –                  | –        | –                  |
| Experiment <sup>b</sup> |              | 1800     |                    |          |                    |          |                    |

<sup>a</sup> EOMIP-CCSD results for  $H_2S$  were taken from Ref. 51.

<sup>b</sup> From Ref. 107

to 50% from EOMIP-CCSD, but at least of the right order of magnitude. Also, the trend in the width going from  $H_2S$  over  $PH_3$  to  $SiH_4$  is correctly captured with MP2-mod.

## B. Partial decay widths

Partial widths for the  $L_{2,3}M$  Coster-Kronig decay channels of hydrogen sulfide computed with MP2, MP2-mod, and EOMIP-CCSD are shown in Tab. XII. The corresponding results for phosphine and silane and for the MM decay channels can be found in the Supporting Information.

The  $L_{2,3}M$  partial widths computed with the MP2-mod method add up to 2090 meV, which is 50% larger than the EOMIP-CCSD result. The width of almost every decay channel is overestimated, but the extent of the overestimation varies considerably between 15 and 70%. However, the dominance of the  $L_{2,3}M$  decay channels (97%) over the MM decay channels (3%) is captured correctly and the branching ratio between singlet and triplet channels (77% vs. 23%) is also in agreement with EOMIP-CCSD (76% vs. 24%). We note that there is a substantial disagreement between our singlet-triplet branching ratios for hydrogen sulfide and those computed with multiconfigurational Dirac-Hartree-Fock theory for the argon atom (45% vs. 55%),<sup>111</sup> which has similar electronic structure.

With the conventional MP2 method the majority of the partial widths in Tab. XII are completely unphysical. Many open channels including those for which the largest widths are expected have zero decay width. This has the same reason as the wrong total widths of  $PH_3$  and  $SiH_4$  discussed in the previous section, namely the orbital energies of the  $L_1$ -edge ionized HF wave function (see Tab. I).

At the same time, the widths of a few other channels are overestimated by MP2. In particular, the  $^1A_1$  ( $1b_12b_1$ ) channel has a width of 19060 meV, which is responsible for the erroneous total width in Tab. XI. We examined this channel further by analyzing the contributions of individual virtual orbitals to Eq. (9). Most of the 19060 meV can be traced back to one single summand where the denominator in Eq. (9) assumes a value of  $-0.0005 - 0.0008i$  a.u., i.e., almost zero.

The respective orbital energies are in atomic units  $\epsilon_{1b_1^\beta} = -7.5166 + 0.0000008i$ ,  $\epsilon_{2b_1^\alpha} = -0.8261 - 0.000004i$ ,  $\epsilon(\text{core hole})_{2a_1^\beta} = -8.2654 + 0.000006i$ , and  $\epsilon_{8a_1^\alpha} = -0.0768 - 0.000844i$ .

The occurrence of such near-singularities depends on the virtual orbital energies, which in turn strongly depend on the basis set. For  $PH_3$  and  $SiH_4$ , no near-singularities occur so that the basis-set dependence of the respective MP2 results in Tab. XI remains inconspicuous.

## C. LLM Coster-Kronig spectra

The LLM Coster-Kronig spectra for hydrogen sulfide, phosphine, and silane computed with the MP2-mod method are shown in Fig. 4. The FWHM is 1.5 eV for all spectra and for  $H_2S$  our spectrum is shifted to higher energies by 2.9 eV. Hydrogen sulfide is the only molecule for which an experimental spectrum is available.<sup>107</sup> In addition, we previously computed this spectrum with EOMIP-CCSD.<sup>51</sup>

The spectrum for  $H_2S$  illustrates good agreement between MP2-mod and EOMIP-CCSD even though the corresponding partial widths (Tab. XII) deviate substantially. The relative intensity of the signal around 25 eV, which is formed by the  $L_{2,3}M_1$  decay channels, is slightly underestimated with MP2-mod, but the feature between 35 eV and 45 eV, which is formed by the  $L_{2,3}M_{2,3}$  decay channels, is obtained with a shape that is almost identical to the EOMIP-CCSD spectrum.

The experimental spectrum is incomplete and only covers the region above 35 eV, where it shows two major signals, a broader one between 37 eV and 39 eV and a sharper one at 42 eV. While this is in line with our computed spectra, the relative intensities are not in agreement. Also, the experimental spectrum includes some further signals with weaker intensity at higher energies (45-50 eV) that the computed spectra lack. We tentatively assign them to resonant decay of core-excited states.

Note that we suggested a different assignment in our previous work (Ref. 51). There, we assigned the peaks with the highest intensity in the experimental spectrum and the com-

TABLE XII. Partial Coster-Kronig decay widths of  $L_1$ -edge ionized hydrogen sulfide computed with CBF-MP2 and ACP-EOMIP-CCSD in the aug-cc-pCVTZ(5sp) basis set with different numbers of complex-scaled s, p, and d-shells added. All values in meV.

| Decay channel  | EOMIP -CCSD <sup>a</sup> | MP2-mod <sup>b</sup> | MP2 <sup>c</sup> |
|--|--------------------------|----------------------|------------------|
| <sup>1</sup> B <sub>1</sub> (4a <sub>1</sub> <sup>-1</sup> 1b <sub>1</sub> <sup>-1</sup> ) | 244.3                    | 281.7                | 0.0              |
| <sup>1</sup> A <sub>1</sub> (3a <sub>1</sub> <sup>-1</sup> 4a <sub>1</sub> <sup>-1</sup> ) | 236.4                    | 288.1                | 0.0              |
| <sup>1</sup> B <sub>2</sub> (4a <sub>1</sub> <sup>-1</sup> 1b <sub>2</sub> <sup>-1</sup> ) | 208.7                    | 326.3                | 0.0              |
| <sup>1</sup> A <sub>1</sub> (1b <sub>1</sub> <sup>-1</sup> 2b <sub>1</sub> <sup>-1</sup> ) | 97.8                     | 155.4                | 19060.3          |
| <sup>1</sup> A <sub>1</sub> (3a <sub>1</sub> <sup>-1</sup> 5a <sub>1</sub> <sup>-1</sup> ) | 97.2                     | 166.0                | 0.1              |
| <sup>3</sup> A <sub>1</sub> (1b <sub>1</sub> <sup>-1</sup> 2b <sub>1</sub> <sup>-1</sup> ) | 76.1                     | 85.0                 | 191.0            |
| <sup>1</sup> A <sub>1</sub> (1b <sub>2</sub> <sup>-1</sup> 2b <sub>2</sub> <sup>-1</sup> ) | 65.2                     | 111.7                | 0.0              |
| <sup>3</sup> A <sub>1</sub> (1b <sub>2</sub> <sup>-1</sup> 2b <sub>2</sub> <sup>-1</sup> ) | 59.8                     | 76.4                 | 0.0              |
| <sup>3</sup> A <sub>1</sub> (3a <sub>1</sub> <sup>-1</sup> 5a <sub>1</sub> <sup>-1</sup> ) | 57.3                     | 79.0                 | 0.1              |
| <sup>1</sup> B <sub>1</sub> (5a <sub>1</sub> <sup>-1</sup> 1b <sub>1</sub> <sup>-1</sup> ) | 43.0                     | 73.1                 | 0.2              |
| <sup>3</sup> B <sub>2</sub> (3a <sub>1</sub> <sup>-1</sup> 2b <sub>2</sub> <sup>-1</sup> ) | 34.1                     | 41.6                 | -0.1             |
| <sup>1</sup> B <sub>2</sub> (5a <sub>1</sub> <sup>-1</sup> 1b <sub>2</sub> <sup>-1</sup> ) | 33.6                     | 64.9                 | 0.1              |
| <sup>3</sup> A <sub>2</sub> (1b <sub>2</sub> <sup>-1</sup> 2b <sub>1</sub> <sup>-1</sup> ) | 32.6                     | 36.3                 | 60.5             |
| <sup>3</sup> B <sub>1</sub> (3a <sub>1</sub> <sup>-1</sup> 2b <sub>1</sub> <sup>-1</sup> ) | 32.2                     | 34.4                 | 53.8             |
| <sup>3</sup> A <sub>2</sub> (2b <sub>2</sub> <sup>-1</sup> 1b <sub>1</sub> <sup>-1</sup> ) | 30.6                     | 41.7                 | 0.0              |
| <sup>3</sup> B <sub>1</sub> (5a <sub>1</sub> <sup>-1</sup> 1b <sub>1</sub> <sup>-1</sup> ) | 26.7                     | 35.3                 | 0.4              |
| <sup>3</sup> B <sub>2</sub> (5a <sub>1</sub> <sup>-1</sup> 1b <sub>2</sub> <sup>-1</sup> ) | 22.9                     | 35.0                 | -4.5             |
| <sup>1</sup> B <sub>2</sub> (3a <sub>1</sub> <sup>-1</sup> 2b <sub>2</sub> <sup>-1</sup> ) | 9.2                      | 39.4                 | -0.1             |
| <sup>1</sup> A <sub>2</sub> (2b <sub>2</sub> <sup>-1</sup> 1b <sub>1</sub> <sup>-1</sup> ) | 8.8                      | 39.2                 | 0.0              |
| <sup>1</sup> A <sub>2</sub> (1b <sub>2</sub> <sup>-1</sup> 2b <sub>1</sub> <sup>-1</sup> ) | 8.3                      | 33.0                 | 14.7             |
| <sup>1</sup> B <sub>1</sub> (3a <sub>1</sub> <sup>-1</sup> 2b <sub>1</sub> <sup>-1</sup> ) | 6.3                      | 31.3                 | 66.6             |
| <sup>3</sup> B <sub>1</sub> (4a <sub>1</sub> <sup>-1</sup> 1b <sub>1</sub> <sup>-1</sup> ) | -5.3                     | 3.6                  | 0.0              |
| <sup>3</sup> A <sub>1</sub> (3a <sub>1</sub> <sup>-1</sup> 4a <sub>1</sub> <sup>-1</sup> ) | -13.7                    | 5.9                  | 0.0              |
| <sup>3</sup> B <sub>2</sub> (4a <sub>1</sub> <sup>-1</sup> 1b <sub>2</sub> <sup>-1</sup> ) | -15.6                    | 5.4                  | 0.0              |
| Sum  | 1396.5                   | 2089.7               | 19443.1          |

<sup>a</sup> From Ref. 51. The basis set is aug-cc-pCVTZ(5sp)+8(spd).

<sup>b</sup> This work. The basis set is aug-cc-pCVTZ(5sp)+8(spd).

<sup>c</sup> This work. The basis set is aug-cc-pCVTZ(5sp)+5(spd).

puted spectrum to each other. With this alternative assignment, there are no unassigned signals at higher energy. However, a large shift of the computed spectrum by 7.5 eV was required to match the experimental spectrum and the feature below 40 eV remained unassigned. Therefore, we believe that the current assignment as shown in Fig. 4 is more sensible.

As concerns phosphine and silane, Fig. 4 shows that the emitted Coster-Kronig electrons have lower energies than for hydrogen sulfide, while the spectra have a similar shape. For all three molecules, the lower-energy peak formed by the  $L_{2,3}M_1$  decay channels is more intense than the higher-energy signals corresponding to the  $L_{2,3}M_{2,3}$  decay channels. The spacing between the two signals shrinks from 12 eV ( $H_2S$ ) over 11 eV ( $PH_3$ ) to 8 eV ( $SiH_4$ ), reflecting the decreasing energy difference between the 3s ( $M_1$ ) and 3p ( $M_{2,3}$ ) orbitals. Also, the higher-energy signal consists of one peak in  $SiH_4$ , while there are two peaks in  $PH_3$  and three in  $H_2S$ . This reflects the degeneracy of the highest occupied molecular orbital in  $SiH_4$  ( $t_2$ ), whereas there are two and three corresponding energy levels in  $PH_3$  and  $H_2S$ , respectively.

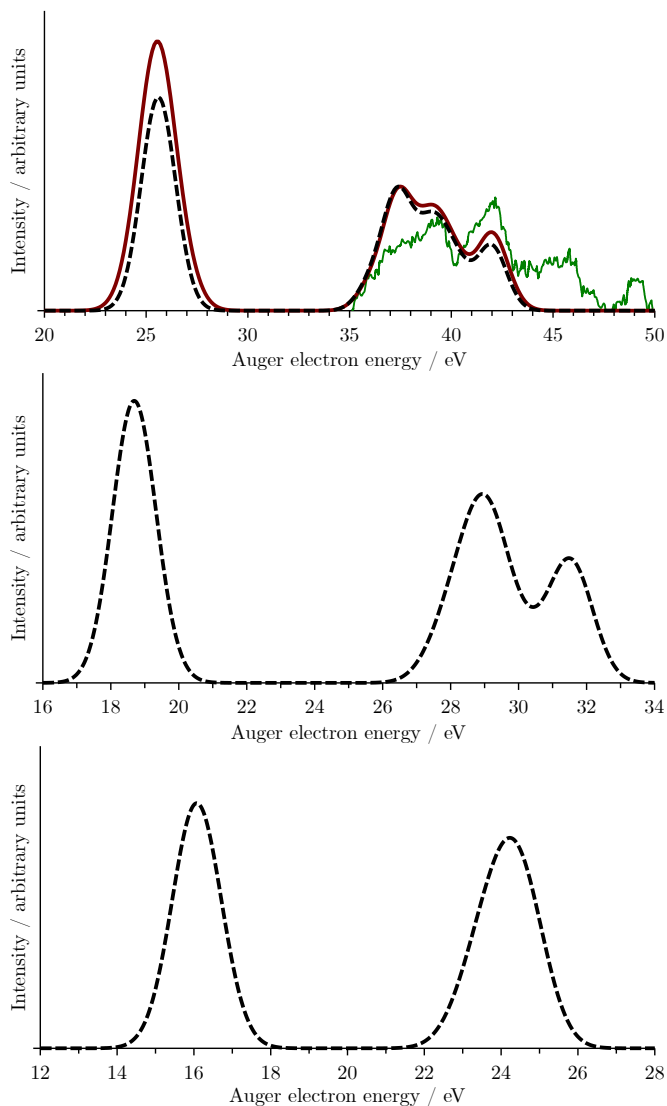


FIG. 4. Coster-Kronig spectra of hydrogen sulfide (top), phosphine (middle), and silane (bottom). Black dashed line: CBF-MP2-mod/EOMDIP-CCSD(2), red line: ACP-EOMIP-CCSD/EOMDIP-CCSD,<sup>51</sup> green line: experiment.<sup>107</sup>

## VII. Conclusions

In this work, we presented an approach for the computation of Auger and Coster-Kronig spectra in the framework of MP2 theory combined with complex-scaled basis functions (CBFs). Based on our earlier work about complex-scaled CCSD,<sup>27</sup> we showed how total and partial decay widths can be computed from the complex-valued MP2 energy of core-ionized states.

We applied this approach to the decay of K and  $L_1$ -ionized states of  $H_2O$ ,  $NH_3$ ,  $CH_4$ ,  $H_2S$ ,  $PH_3$ , and  $SiH_4$ . For K-edge decay of  $H_2S$ ,  $PH_3$ , and  $SiH_4$ , CBF-MP2 works very well. The dominance of the LL decay channels (>90%) over LM (1–10%) and MM (<1%) decay channels is captured correctly and the RMS deviation of the individual partial decay widths from CBF-CCSD amounts to only 0.5 meV.

For the corresponding decay processes in  $H_2O$ ,  $NH_3$ , and

CH<sub>4</sub>, CBF-MP2 performs significantly worse with the RMS deviation of the individual partial decay widths from CBF-CCSD amounting to 4 meV. The widths of some channels are overestimated by 50% resulting in a too large total width and distorted branching ratios.

For Coster-Kronig decay of L<sub>1</sub>-ionized states of H<sub>2</sub>S, PH<sub>3</sub>, and SiH<sub>4</sub>, CBF-MP2 fails completely. We traced this back to the fact that L<sub>2,3</sub>M decay channels are closed in the HF wave functions of L<sub>1</sub>-ionized states. By using orbital energies from the HF wave functions of the corresponding neutral states in the MP2 energy expression, qualitatively correct results can be obtained for decay of L<sub>1</sub>-ionized states. Moreover, the description of the decay of K-ionized states of H<sub>2</sub>O, NH<sub>3</sub>, and CH<sub>4</sub> is improved somewhat as well.

To describe the final states of Auger decay, we introduced in this work a double ionization potential variant of the EOM-CCSD(2) method,<sup>83</sup> also known as EOM-MP2. The double ionization energies computed with this method show an RMS deviation from EOMDIP-CCSD that amounts to 0.08 eV for H<sub>2</sub>O, NH<sub>3</sub>, and CH<sub>4</sub> and to 0.38 eV for H<sub>2</sub>S, PH<sub>3</sub>, and SiH<sub>4</sub>, which is acceptable for most purposes in the context of Auger spectroscopy.

Taken together, the construction of Auger spectra from CBF-MP2 and EOMDIP-CCSD(2) calculations entails substantially lower computational cost than our previous approach based on CBF-CCSD and EOMDIP-CCSD without compromising accuracy. At the same time, the need to shift the orbital energy denominator for some states limits the viability of the CBF-MP2 method. This shortcoming is avoided in an EOM-CC approach in which all states relevant to Auger decay are built from the same reference wave function that is optimized for the neutral molecule.<sup>48</sup>

The comparison of the Auger spectra computed in this work to experimental data shows overall good agreement regarding peak positions and intensities, but also illustrates the impact of effects that are not included in our current theoretical approach. For example, the impact of nuclear motion is rather prominent in the Auger spectrum of water and spin-orbit effects are visible for hydrogen sulfide. We also hope that the LLM Coster-Kronig spectra of PH<sub>3</sub> and SiH<sub>4</sub> and the KLM spectrum of H<sub>2</sub>S presented in our work foster measurements of these spectra.

### Acknowledgments

T.-C. J. gratefully acknowledges funding from the European Research Council (ERC) under the European Union's Horizon 2020 research and innovation program (Grant Agreement No. 851766) and the KU Leuven internal funds (Grant No. C14/22/083). The authors are grateful to Prof. Sonia Coriani for helpful comments regarding the errors in the core-ionization energies due to relativistic effects.

### Data Availability Statement

The data that supports the finding of this study are available within the article and its supplementary material.

### References

- <sup>1</sup>Auger, P. Sur les rayons  $\beta$  secondaires produits dans un gaz par des rayons X. *CR Acad. Sci. (F)* **1923**, 177, 169.
- <sup>2</sup>Rennie, E. E.; Kempgens, B.; Köppe, H. M.; Hergenhanh, U.; Feldhaus, J.; Itchkawitz, B. S.; Kilcoyne, A. L. D.; Kivimäki, A.; Maier, K.; Piancastelli, M. N.; Polcik, M.; Rüdél, A.; Bradshaw, A. M. A comprehensive photoabsorption, photoionization, and shake-up excitation study of the C 1s cross section of benzene. *J. Chem. Phys.* **2000**, 113, 7362.
- <sup>3</sup>Carniato, S. et al. Single photon simultaneous K-shell ionization/excitation in C<sub>6</sub>H<sub>6</sub>: Experiment and theory. *J. Phys. B.: At. Mol. Opt.* **2020**, 53, 244010.
- <sup>4</sup>Spohr, R.; Bergmark, T.; Magnusson, N.; Werme, L.; Nordling, C.; Siegbahn, K. Electron Spectroscopic Investigation of Auger Processes in Bromine Substituted Methanes and Some Hydrocarbons. *Phys. Scripta* **1970**, 2, 31.
- <sup>5</sup>Loveland, W. D.; Morrissey, D. J.; Seaborg, G. T. *Modern nuclear chemistry*; John Wiley & Sons, 2017.
- <sup>6</sup>Rye, R. R.; Houston, J. E. Molecular Auger spectroscopy. *Acc. Chem. Res.* **1984**, 17, 41.
- <sup>7</sup>Bolognesi, P.; O'Keeffe, P.; Ovcharenko, Y.; Avaldi, L.; Carravetta, V. Resonant Auger spectroscopy at the carbon and nitrogen K-edges of pyrimidine. *J. Chem. Phys.* **2012**, 136, 154308.
- <sup>8</sup>Agarwal, B. K. *X-ray spectroscopy: An introduction*; Springer, 2013.
- <sup>9</sup>McFarland, B. K. et al. Ultrafast X-ray Auger probing of photoexcited molecular dynamics. *Nat. Commun.* **2014**, 5, 4235.
- <sup>10</sup>Ramasesha, K.; Leone, S. R.; Neumark, D. M. Real-time probing of electron dynamics using attosecond time-resolved spectroscopy. *Annu. Rev. Phys. Chem.* **2016**, 67, 41.
- <sup>11</sup>Nisoli, M.; Decleva, P.; Calegari, F.; Palacios, A.; Martín, F. Attosecond Electron Dynamics in Molecules. *Chem. Rev.* **2017**, 117, 10760.
- <sup>12</sup>Marchenko, T.; Inhester, L.; Goldsztejn, G.; Travnikova, O.; Journal, L.; Guillemin, R.; Ismail, I.; Koulentianos, D.; Céolin, D.; Püttner, R.; Piancastelli, M. N.; Simon, M. Ultrafast nuclear dynamics in the doubly-core-ionized water molecule observed via Auger spectroscopy. *Phys. Rev. A* **2018**, 98, 063403.
- <sup>13</sup>Norman, P.; Dreuw, A. Simulating X-ray Spectroscopies and Calculating Core-Excited States of Molecules. *Chem. Rev.* **2018**, 118, 7208.
- <sup>14</sup>Kraus, P. M.; Zürich, M.; Cushing, S. K.; Neumark, D. M.; Leone, S. R. The ultrafast X-ray spectroscopy revolution in chemical dynamics. *Nat. Rev. Chem.* **2018**, 2, 82.
- <sup>15</sup>Plekan, O. et al. Experimental and theoretical photoemission study of indole and its derivatives in the gas phase. *J. Phys. Chem. A* **2020**, 124, 4115.
- <sup>16</sup>Tchaplyguine, M.; Feifel, R.; Marinho, R. R. T.; Gisselbrecht, M.; Sorensen, S. L.; de Brito, A. N.; Mårtensson, N.; Svensson, S.; Björneholm, O. Selective probing of the electronic structure of free clusters using resonant core-level spectroscopy. *Chem. Phys.* **2003**, 289, 3.
- <sup>17</sup>Chao, L.-C.; Yang, S.-H. Growth and Auger electron spectroscopy characterization of donut-shaped ZnO nanostructures. *Appl. Surf. Sci.* **2007**, 253, 7162.
- <sup>18</sup>Raman, S. N.; Paul, D. F.; Hammond, J. S.; Bomben, K. D. Auger electron spectroscopy and its application to nanotechnology. *Microsc. today* **2011**, 19, 12.
- <sup>19</sup>Ku, A.; Facca, V. J.; Cai, Z.; Reilly, R. M. Auger electrons for cancer therapy—a review. *EJNMMI Radiopharm. Chem.* **2019**, 4, 1.
- <sup>20</sup>Pirovano, G.; Wilson, T. C.; Reiner, T. Auger: The future of precision medicine. *Nucl. Med. Biol.* **2021**, 96, 50.
- <sup>21</sup>Hanke, G.; Müller, K. A comparison of low energy Auger spectra of the nitrides and oxides of the light elements lithium, beryllium and boron. *Surface Science* **1985**, 152-153, 902.
- <sup>22</sup>Li, Z.; Becker, U. Chemical state effects on the Auger transitions in Cr, Fe, and Cu compounds. *J. Electron. Spectrosc. Relat. Phenom.* **2019**, 237, 146893.
- <sup>23</sup>Hofmann, S. *Auger- and X-ray photoelectron spectroscopy in materials science: A user-oriented guide*; Springer Science & Business Media, 2012; Vol. 49.
- <sup>24</sup>Orvis, T.; Surendran, M.; Liu, Y.; Cunniff, A.; Ravichandran, J. In situ Auger electron spectroscopy of complex oxide surfaces grown by pulsed laser deposition. *J. Vac. Sci. Technol., A* **2019**, 37, 061401.
- <sup>25</sup>Fransson, T.; Harada, Y.; Kosugi, N.; Besley, N. A.; Winter, B.; Rehr, J. J.; Pettersson, L. G. M.; Nilsson, A. X-ray and Electron Spectroscopy of Water. *Chem. Rev.* **2016**, 116, 7551.
- <sup>26</sup>Moiseyev, N. *Non-Hermitian quantum mechanics*; Cambridge University Press, 2011.

- <sup>27</sup>Matz, F.; Jagau, T.-C. Molecular Auger decay rates from complex-variable coupled-cluster theory. *J. Chem. Phys.* **2022**, *156*, 114117.
- <sup>28</sup>Jagau, T.-C. Theory of electronic resonances: fundamental aspects and recent advances. *Chem. Comm.* **2022**, *58*, 5205.
- <sup>29</sup>Fano, U. Effects of configuration interaction on intensities and phase shifts. *Phys. Rev.* **1961**, *124*, 1866.
- <sup>30</sup>Feshbach, H. A unified theory of nuclear reactions. II. *Ann. Phys.* **1962**, *19*, 287.
- <sup>31</sup>Löwdin, P.-O. Studies in perturbation theory. IV. Solution of eigenvalue problem by projection operator formalism. *J. Math. Phys.* **1962**, *3*, 969.
- <sup>32</sup>Averbukh, V.; Cederbaum, L. S. Ab initio calculation of interatomic decay rates by a combination of the Fano ansatz, Green's-function methods, and the Stieltjes imaging technique. *J. Chem. Phys.* **2005**, *123*, 204107.
- <sup>33</sup>Inhester, L.; Burmeister, C. F.; Groenhof, G.; Grubmüller, H. Auger spectrum of a water molecule after single and double core ionization. *J. Chem. Phys.* **2012**, *136*, 144304.
- <sup>34</sup>Inhester, L.; Burmeister, C. F.; Groenhof, G.; Grubmüller, H. Erratum: "Auger spectrum of a water molecule after single and double core ionization" [J. Chem. Phys. 136, 144304 (2012)]. *J. Chem. Phys.* **2014**, *141*, 069904.
- <sup>35</sup>Kolorenč, P.; Averbukh, V. Fano-ADC(2,2) method for electronic decay rates. *J. Chem. Phys.* **2020**, *152*, 214107.
- <sup>36</sup>Skomorowski, W.; Krylov, A. I. Feshbach–Fano approach for calculation of Auger decay rates using equation-of-motion coupled-cluster wave functions. I. Theory and implementation. *J. Chem. Phys.* **2021**, *154*, 084124.
- <sup>37</sup>Skomorowski, W.; Krylov, A. I. Feshbach–Fano approach for calculation of Auger decay rates using equation-of-motion coupled-cluster wave functions. II. Numerical examples and benchmarks. *J. Chem. Phys.* **2021**, *154*, 084125.
- <sup>38</sup>Gorczyca, T. W. Auger decay of the photoexcited  $1s^{-1}np$  Rydberg series in neon. *Phys. Rev. A* **2000**, *61*, 024702.
- <sup>39</sup>García, J.; Kallman, T. R.; Witthoef, M.; Behar, E.; Mendoza, C.; Palmeri, P.; Quinet, P.; Bautista, M. A.; Klapisch, M. Nitrogen K-Shell Photoabsorption. *Astrophys. J. Suppl. S.* **2009**, *185*, 477.
- <sup>40</sup>Carravetta, V.; Ågren, H. Stieltjes imaging method for molecular Auger transition rates: Application to the Auger spectrum of water. *Phys. Rev. A* **1987**, *35*, 1022.
- <sup>41</sup>Cederbaum, L. S.; Domcke, W.; Schirmer, J. Many-body theory of core holes. *Phys. Rev. A* **1980**, *22*, 206.
- <sup>42</sup>Coriani, S.; Koch, H. Communication: X-ray absorption spectra and core-ionization potentials within a core-valence separated coupled cluster framework. *J. Chem. Phys.* **2015**, *143*, 181103.
- <sup>43</sup>Vidal, M. L.; Feng, X.; Epifanovsky, E.; Krylov, A. I.; Coriani, S. New and Efficient Equation-of-Motion Coupled-Cluster Framework for Core-Excited and Core-Ionized States. *J. Chem. Theory Comput.* **2019**, *15*, 3117.
- <sup>44</sup>Siegbahn, H.; Asplund, L.; Kelfve, P. The Auger electron spectrum of water vapour. *Chem. Phys. Lett.* **1975**, *35*, 330.
- <sup>45</sup>Grell, G.; Bokarev, S. I. Multi-reference protocol for (auto)ionization spectra: Application to molecules. *J. Chem. Phys.* **2020**, *152*, 074108.
- <sup>46</sup>Gerlach, M.; Preitschopf, T.; Karaev, E.; Quidián-Lara, H. M.; Mayer, D.; Bozek, J.; Fischer, I.; Fink, R. F. Auger electron spectroscopy of fulminic acid, HCNO: an experimental and theoretical study. *Phys. Chem. Chem. Phys.* **2022**, *24*, 15217–15229.
- <sup>47</sup>Tenorio, B. N. C.; Voß, T. A.; Bokarev, S. I.; Decleva, P.; Coriani, S. Multireference approach to normal and resonant Auger spectra based on the one-center approximation. *J. Chem. Theory Comput.* **2022**, *18*, 4387.
- <sup>48</sup>Matz, F.; Jagau, T.-C. Channel-specific core-valence projectors for determining partial Auger decay widths. *Mol. Phys.* **2023**, *121*, e2105270.
- <sup>49</sup>Matz, F.; Nijssen, J.; Jagau, T.-C. Ab initio investigation of the Auger spectra of methane, ethane, ethylene, and acetylene. *J. Phys. Chem. A* **2023**, *127*, 6147.
- <sup>50</sup>Jayadev, N. K.; Ferino-Pérez, A.; Matz, F.; Krylov, A. I.; Jagau, T.-C. The Auger spectrum of benzene. *J. Chem. Phys.* **2023**, *158*, 064109.
- <sup>51</sup>Drennhaus, J. P.; Ferino-Pérez, A.; Matz, F.; Jagau, T. C. Ab initio treatment of molecular Coster-Kronig decay using complex-scaled equation-of-motion coupled-cluster theory. *Phys. Chem. Chem. Phys.* **2024**, *26*, 23846.
- <sup>52</sup>Ferino-Pérez, A.; Jagau, T.-C. Ab Initio Computation of Auger Decay in Heavy Metals: Zinc about It. *J. Phys. Chem. A* **2024**, *128*, 3957–3967.
- <sup>53</sup>Aguilar, J.; Combes, J.-M. A class of analytic perturbations for one-body Schrödinger Hamiltonians. *Commun. Math. Phys.* **1971**, *22*, 269.
- <sup>54</sup>Balslev, E.; Combes, J.-M. Spectral properties of many-body Schrödinger operators with dilatation-analytic interactions. *Commun. Math. Phys.* **1971**, *22*, 280.
- <sup>55</sup>McCurdy Jr, C. W.; Rescigno, T. N. Extension of the method of complex basis functions to molecular resonances. *Phys. Rev. Lett.* **1978**, *41*, 1364.
- <sup>56</sup>Moiseyev, N.; Corcoran, C. Autoionizing states of  $H_2$  and  $H_2^-$  using the complex-scaling method. *Phys. Rev. A* **1979**, *20*, 814.
- <sup>57</sup>Bravaya, K. B.; Zuev, D.; Epifanovsky, E.; Krylov, A. I. Complex-scaled equation-of-motion coupled-cluster method with single and double substitutions for autoionizing excited states: Theory, implementation, and examples. *J. Chem. Phys.* **2013**, *138*, 124106.
- <sup>58</sup>Jagau, T.-C.; Zuev, D.; Bravaya, K. B.; Epifanovsky, E.; Krylov, A. I. A Fresh Look at Resonances and Complex Absorbing Potentials: Density Matrix-Based Approach. *J. Phys. Chem. Lett.* **2014**, *5*, 310.
- <sup>59</sup>Zuev, D.; Jagau, T.-C.; Bravaya, K. B.; Epifanovsky, E.; Shao, Y.; Sundstrom, E.; Head-Gordon, M.; Krylov, A. I. Complex absorbing potentials within EOM-CC family of methods: Theory, implementation, and benchmarks. *J. Chem. Phys.* **2014**, *141*, 024102.
- <sup>60</sup>White, A. F.; Head-Gordon, M.; McCurdy, C. W. Complex basis functions revisited: Implementation with applications to carbon tetrafluoride and aromatic N-containing heterocycles within the static-exchange approximation. *J. Chem. Phys.* **2015**, *142*, 054103.
- <sup>61</sup>White, A. F.; McCurdy, C. W.; Head-Gordon, M. Restricted and unrestricted non-Hermitian Hartree-Fock: Theory, practical considerations, and applications to metastable molecular anions. *J. Chem. Phys.* **2015**, *143*, 074103.
- <sup>62</sup>White, A. F.; Epifanovsky, E.; McCurdy, C. W.; Head-Gordon, M. Second order Möller-Plesset and coupled cluster singles and doubles methods with complex basis functions for resonances in electron-molecule scattering. *J. Chem. Phys.* **2017**, *146*, 234107.
- <sup>63</sup>Jagau, T.-C.; Bravaya, K. B.; Krylov, A. I. Extending Quantum Chemistry of Bound States to Electronic Resonances. *Annu. Rev. Phys. Chem.* **2017**, *525*.
- <sup>64</sup>Triguero, L.; Plashkevych, O.; Pettersson, L. G. M.; Ågren, H. Separate state vs. transition state Kohn-Sham calculations of X-ray photoelectron binding energies and chemical shifts. *J. Electron Spectrosc. Relat. Phenom.* **1999**, *104*, 195.
- <sup>65</sup>Duflot, D.; Flament, J.-P.; Heinesch, J.; Hubin-Franskin, M.-J. The K-shell spectra of tetrahydrofuran studied by electron energy loss spectroscopy and abinitio calculations. *Chem. Phys. Lett.* **2010**, *495*, 27–32.
- <sup>66</sup>Shim, J.; Klobukowski, M.; Barysz, M.; Leszczynski, J. Calibration and applications of the  $\Delta MP2$  method for calculating core electron binding energies. *Phys. Chem. Chem. Phys.* **2011**, *13*, 5703–5711.
- <sup>67</sup>Ljubić, I. Reliability of Density Functional and Perturbation Theories for Calculating Core-Ionization Spectra of Free Radicals. *J. Chem. Theory Comput.* **2014**, *10*, 2333–2343.
- <sup>68</sup>Kovač, B.; Ljubić, I.; Kivimäki, A.; Coreno, M.; Novak, I. Characterisation of the electronic structure of some stable nitroxyl radicals using variable energy photoelectron spectroscopy. *Phys. Chem. Chem. Phys.* **2014**, *16*, 10734–10742.
- <sup>69</sup>Su, N. Q.; Xu, X. Second-Order Perturbation Theory for Fractional Occupation Systems: Applications to Ionization Potential and Electron Affinity Calculations. *J. Chem. Theory Comput.* **2016**, *12*, 2285–2297.
- <sup>70</sup>Šmiga, S.; Grabowski, I. Spin-Component-Scaled  $\Delta MP2$  Parametrization: Toward a Simple and Reliable Method for Ionization Energies. *J. Chem. Theory Comput.* **2018**, *14*, 4780–4790.
- <sup>71</sup>Nooijen, M.; Bartlett, R. J. Similarity transformed equation-of motion coupled-cluster theory: Details, examples, and comparisons. *J. Chem. Phys.* **1997**, *107*, 6812–6830.
- <sup>72</sup>Sattelmeyer, K. W.; Schaefer, H. F.; Stanton, J. F. Use of 2h and 3h-p like coupled-cluster Tamm-Dancoff approaches for the equilibrium properties of ozone. *Chem. Phys. Lett.* **2003**, *378*, 42–46.
- <sup>73</sup>Siegert, A. J. F. On the derivation of dispersion formula for nuclear reactions. *Phys. Rev.* **1939**, *56*, 750.
- <sup>74</sup>Camps, S.; Utku, C.; Creutzberg, J.; Jagau, T.-C. Complex-variable equation-of-motion coupled-cluster singles and doubles theory with the resolution-of-the-identity approximation. *J. Phys. Chem. A* **2025**, *submit*-*ted*.

- <sup>75</sup>Creutzberg, J.; Skomorowski, W.; Jagau, T.-C. Computing decay widths of autoionizing Rydberg states with complex-variable coupled-cluster theory. *J. Phys. Chem. Lett.* **2023**, *14*, 10943–10950.
- <sup>76</sup>Parravicini, V.; Jagau, T.-C. Interatomic and intermolecular Coulombic decay rates from equation-of-motion coupled-cluster theory with complex basis functions. *J. Chem. Phys.* **2023**, *159*, 094112.
- <sup>77</sup>Jagau, T.-C. Coupled-cluster treatment of molecular strong-field ionization. *J. Chem. Phys.* **2018**, *148*, 204102/1–9.
- <sup>78</sup>Hernández Vera, M.; Jagau, T.-C. Resolution-of-the-identity approximation for complex-scaled basis functions. *J. Chem. Phys.* **2019**, *151*.
- <sup>79</sup>Bartlett, R. J. Coupled-cluster theory and its equation-of-motion extensions. *WIREs Comput. Mol. Sci.* **2012**, *2*, 126.
- <sup>80</sup>Sneskov, K.; Christiansen, O. Excited state coupled cluster methods. *WIREs Comput. Mol. Sci.* **2012**, *2*, 566.
- <sup>81</sup>Moiseyev, N.; Certain, P.; Weinhold, F. Resonance properties of complex-rotated Hamiltonians. *Mol. Phys.* **1978**, *36*, 1613.
- <sup>82</sup>Chase, R. L.; Kelly, H. P.; Köhler, H. S. Correlation Energies and Auger Rates in Atoms with Inner-Shell Vacancies. *Phys. Rev. A* **1971**, *3*, 1550.
- <sup>83</sup>Stanton, J. F.; Gauss, J. Perturbative treatment of the similarity transformed Hamiltonian in equation-of-motion coupled-cluster approximations. *J. Chem. Phys.* **1995**, *103*, 1064.
- <sup>84</sup>Epifanovsky, E. et al. Software for the frontiers of quantum chemistry: An overview of developments in the Q-Chem 5 package. *J. Chem. Phys.* **2021**, *155*, 084801.
- <sup>85</sup>Wang, P.; Carroll, T. X.; Thomas, T. D.; Sæthre, L. J.; Børve, K. J. Calibration of oxygen 1s ionization energies. Accurate energies for CO<sub>2</sub>, H<sub>2</sub>O, CO, and O<sub>2</sub>. *J. Electron Spectrosc.* **2021**, *251*, 147103.
- <sup>86</sup>Kryzhevoi, N. V.; Cederbaum, L. S. Nonlocal Effects in the Core Ionization and Auger Spectra of Small Ammonia Clusters. *J. Phys. Chem. B* **2011**, *115*, 5441.
- <sup>87</sup>Sæthre, L. J.; Sværen, O.; Svensson, S.; Osborne, S.; Thomas, T. D.; Jauhiainen, J.; Aksela, S. High-resolution C 1s photoelectron spectra of methane, ethene, propene, and 2-methylpropene. *Phys. Rev. A* **1997**, *55*, 2748.
- <sup>88</sup>Carbone, J. P.; Cheng, L.; Myhre, R. H.; Matthews, D.; Koch, H.; Coriani, S. In *State of The Art of Molecular Electronic Structure Computations: Correlation Methods, Basis Sets and More*; Ancarani, L. U., Hoggan, P. E., Eds.; Advances in Quantum Chemistry; Academic Press, 2019; Vol. 79; p 241.
- <sup>89</sup>Sankari, R.; Ehara, M.; Nakatsuji, H.; Senba, Y.; Hosokawa, K.; Yoshida, H.; De Fanis, A.; Tamenori, Y.; Aksela, S.; Ueda, K. Vibrationally resolved O 1s photoelectron spectrum of water. *Chem. Phys. Lett.* **2003**, *380*, 647.
- <sup>90</sup>Carroll, T. X.; Berrah, N.; Bozek, J.; Hahne, J.; Kukk, E.; Sæthre, L. J.; Thomas, T. D. Carbon 1s photoelectron spectrum of methane: Vibrational excitation and core-hole lifetime. *Phys. Rev. A* **1999**, *59*, 3386.
- <sup>91</sup>Carlson, T. A.; Krause, M. O. Experimental evidence for double electron emission in an Auger process. *Phys. Rev. Lett.* **1965**, *14*, 390–392.
- <sup>92</sup>Moddeman, W. E.; Carlson, T. A.; Krause, M. O.; Pullen, B. P.; Bull, W. E.; Schweitzer, G. K. Determination of the K—LL Auger Spectra of N<sub>2</sub>, O<sub>2</sub>, CO, NO, H<sub>2</sub>O, and CO<sub>2</sub>. *J. Chem. Phys.* **1971**, *55*, 2317.
- <sup>93</sup>Shaw Jr., R. W.; Jen, J. S.; Thomas, T. D. Auger spectrum of ammonia. *J. Electron Spectrosc. Relat. Phenom.* **1977**, *11*, 91–100.
- <sup>94</sup>Kivimäki, A.; Neeb, M.; Kempgens, B.; Köppe, H. M.; Bradshaw, A. M. The C 1s Auger decay spectrum of the CH<sub>4</sub> molecule: The effects of vibrational fine structure, double excitations and shake-up transitions. *J. Phys. B – At. Mol. Opt. Phys.* **1996**, *29*, 2701.
- <sup>95</sup>Cederbaum, L. S.; Campos, P.; Tarantelli, F.; Sgamellotti, A. Band shape and vibrational structure in Auger spectra: Theory and application to carbon monoxide. *J. Chem. Phys.* **1991**, *95*, 6634.
- <sup>96</sup>Zheng, X.; Zhang, C.; Jin, Z.; Southworth, S. H.; Cheng, L. Benchmark relativistic delta-coupled-cluster calculations of K-edge core-ionization energies of third-row elements. *Phys. Chem. Chem. Phys.* **2022**, *24*, 13587.
- <sup>97</sup>Keski-Rahkonen, O.; Krause, M. O. Total and partial atomic-level widths. *Atom. Data Nucl. Data* **1974**, *14*, 139.
- <sup>98</sup>Bodeur, S.; Millié, P.; Nenner, I. Single- and multiple-electron effects in the Si 1s photoabsorption spectra of SiX<sub>4</sub> (X=H,D,F,Cl,Br,CH<sub>3</sub>,C<sub>2</sub>H<sub>5</sub>,OCH<sub>3</sub>,OC<sub>2</sub>H<sub>5</sub>) molecules: Experiment and theory. *Phys. Rev. A* **1990**, *41*, 252.
- <sup>99</sup>McGuire, E. J. K-Shell Auger Transition Rates and Fluorescence Yields for Elements Be–Ar. *Phys. Rev.* **1969**, *185*, 1.
- <sup>100</sup>Ågren, H. On the interpretation of molecular valence Auger spectra. *J. Chem. Phys.* **1981**, *75*, 1267.
- <sup>101</sup>Tarantelli, F.; Sgamellotti, A.; Cederbaum, L. S.; Schirmer, J. Theoretical investigation of many dicationic states and the Auger spectrum of benzene. *J. Chem. Phys.* **1987**, *86*, 2201–2206.
- <sup>102</sup>Vayrynen, J.; Sodhi, R. N.; Cavell, R. G. Energies and intensities of the KLL Auger spectra of SiH<sub>4</sub>, PH<sub>3</sub>, HCl, and Ar. *J. Chem. Phys.* **1983**, *79*, 5329.
- <sup>103</sup>Jayadev, N. K.; Skomorowski, W.; Krylov, A. I. Incorporating the effect of spin-orbit interaction in Auger decay spectra: Theory and examples. *J. Chem. Phys.* **2025**, *submitted*.
- <sup>104</sup>Püttner, R.; Céolin, D.; Guillemin, R.; Kushawaha, R. K.; Marchenko, T.; Journel, L.; Piancastelli, M. N.; Simon, M. Detailed analysis of shake structures in the KLL Auger spectrum of H<sub>2</sub>S. *Phys. Rev. A* **2016**, *93*, 042501.
- <sup>105</sup>Faegri Jr, K.; Keski-Rahkonen, O. Sulphur KLL Auger spectra of gaseous sulphur compounds. *J. Electron Spectrosc.* **1977**, *11*, 275.
- <sup>106</sup>Asplund, L.; Kelfve, P.; Blomster, B.; Siegbahn, H.; Siegbahn, K.; Lozes, R. L.; Wahlgren, U. I. Molecular Auger electron spectra of second row elements. Sulfur compounds. *Phys. Scripta* **1977**, *16*, 273.
- <sup>107</sup>Hikosaka, Y.; Lablanquie, P.; Penent, F.; Lambourne, J. G.; Hall, R. I.; Aoto, T.; Ito, K. Sub-natural linewidth Auger electron spectroscopy of the 2s hole decay in H<sub>2</sub>S. *J. Electron Spectrosc.* **2004**, *137*, 287.
- <sup>108</sup>Sodhi, R. N. S.; Brion, C. E. Electronic excitations in phosphorus-containing molecules. I. Inner shell electron energy loss spectra of PH<sub>3</sub>, P(CH<sub>3</sub>)<sub>3</sub>, PF<sub>3</sub> and PCl<sub>3</sub>. *J. Electron Spectrosc. Relat. Phenom.* **1985**, *37*, 97.
- <sup>109</sup>Cooper, G.; Ibuki, T.; Brion, C. E. Absolute oscillator strengths for photoabsorption, photoionization and ionic photofragmentation of silane. II. The Si 2p and 2s inner shells. *Chem. Phys.* **1990**, *140*, 147.
- <sup>110</sup>Coster, D.; de Laer Kronig, R. New type of Auger effect and its influence on the x-ray spectrum. *Physica* **1935**, *2*, 13.
- <sup>111</sup>Liu, Z.; Liu, Q.; Ma, Y.; Zhou, F.; Qu, Y. Influence of orbital sets on the Ar<sup>+</sup>(2s<sup>-1</sup>) multiple Auger decay. *Phys. Rev. A* **2021**, *103*, 063102.